REPORT NO.
UCB/EERC-83/05
MAY 1983

EARTHQUAKE ENGINEERING RESEARCH CENTER

A TRANSDUCER FOR MEASURING THE INTERNAL FORCES IN THE COLUMNS OF A FRAME-WALL REINFORCED CONCRETE STRUCTURE

by

RICHARD SAUSE
V.V. BERTERO

Report to Sponsor:
National Science Foundation

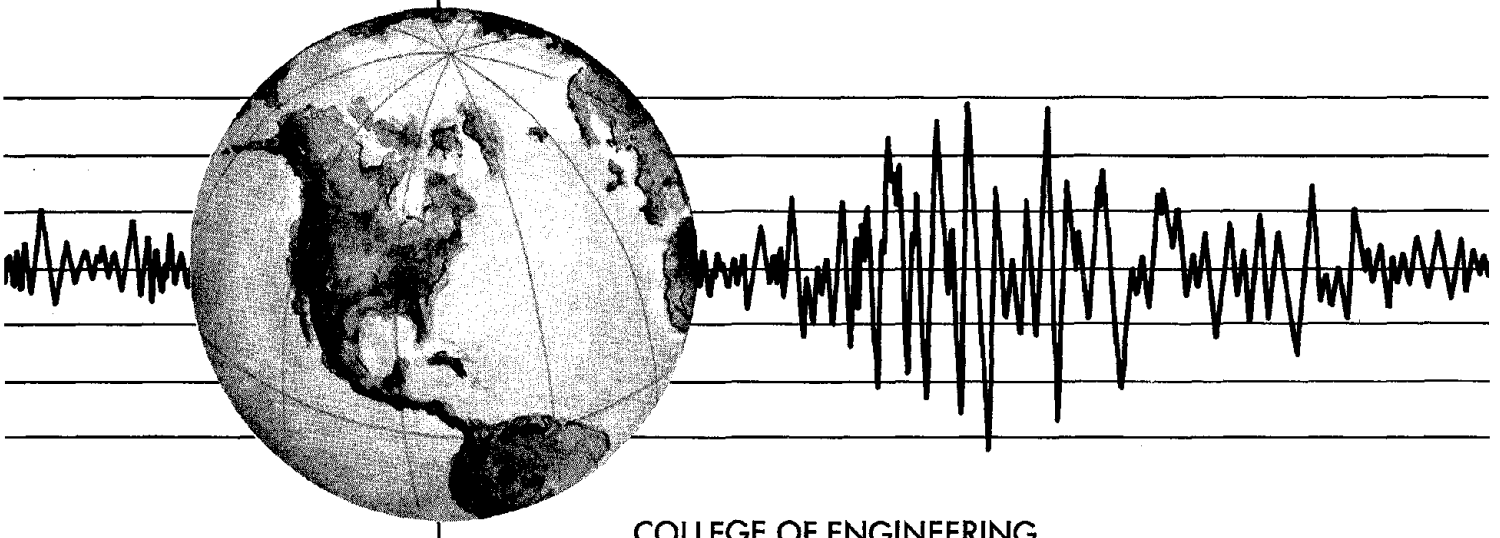

COLLEGE OF ENGINEERING

UNIVERSITY OF CALIFORNIA · Berkeley, California

For sale by the National Technical Information Service, U.S. Department of Commerce, Springfield, Virginia 22161.

See back of report for up to date listing of EERC reports.

A TRANSDUCER FOR MEASURING THE INTERNAL FORCES IN THE COLUMNS OF A FRAME-WALL REINFORCED CONCRETE STRUCTURE

by

Richard Sause
Graduate Student
Department of Civil Engineering
University of California, Berkeley

V. V. Bertero
Professor of Civil Engineering
University of California, Berkeley

Report to Sponsor:
National Science Foundation

Report No. UCB/EERC-83/05
Earthquake Engineering Research Center
College of Engineering
University of California
Berkeley, California

May 1983

ABSTRACT

A transducer capable of accurately measuring the internal forces of the first-story columns of a 1/5 scale model of a seven-story frame-wall reinforced concrete structure has been designed, developed, and applied in this structure under static and dynamic loading conditions. This internal force transducer (IFT) was developed specifically for research on this structure which is part of the U.S.-Japan Cooperative Research Program Utilizing Large-Scale Testing Facilities. However, the feasibility considerations, the development of design criteria, the design and fabrication considerations, and the calibration and installation methods reported herein have more general applicability.

From the results obtained in the calibration of the fabricated IFTs, and during the tests conducted on the 1/5 scale model, it has been concluded that for the primary purpose of studying the dynamic response of the 1/5 scale model to earthquake ground motions, the performance of the IFTs is acceptable. For short term static loading of the 1/5 scale model, their performance is also acceptable. However, as a consequence of contamination of the exposed surface of the applied shear and axial strain gages used in this internal force transducer, there are some long time zero drifts which make analysis of results

obtained under sustained loading conditions or from long time effects (internal force redistribution) difficult.

Recommendations for improving the design, fabrication, calibration and installation of similar internal force transducers are formulated.

ACKNOWLEDGEMENTS

Financial support for this research was provided by the National Science Foundation under Grant No. PFR-8009478. This support is part of the support provided for the U.S.-Japan Cooperative Research Program.

The research reported herein was conducted by Richard Sause as part of his graduate studies under the direction and guidance of Professor V. V. Bertero. The preliminary research conducted by Visiting Professor H. G. Harris and Dr. A. E. Aktan, associate research engineer, and the continued guidance and assistance of Dr. Aktan are acknowledged. Special thanks to Professor J. P. Moehle for his comments on this report. Also thanks to Research Assistants Finley Charney, Abed Chowdhury, and to Amir Said Javadian-Gilani and Stanley Fung.

The special effort of Don Clyde in this research is appreciated. Also the assistance of individuals in the SESM Machine Shop, SESM Electronics Shop, and the RFS Structures Laboratory Machine Shop is acknowledged. Special thanks to A. D. Lawrence and Lou Trescony. Also thanks to Professor D. Pirtz for his help in the use of creep testing apparatus. The dedicated work of Bill Boller of Chalet Tool Inc. is also appreciated.

Typing of this report was done by Joan Clark, Patricia Rorrison, Hannelore Sause, and Katherine Butterfield. The figures were prepared by Richard Steele and the final editing of the report was done by Susan Gardner.

TABLE OF CONTENTS

	Page
ABSTRACT	iii
ACKNOWLEDGEMENTS	v
TABLE OF CONTENTS	vii
LIST OF TABLES	xi
LIST OF FIGURES	xiii
1. INTRODUCTION	1
1.1 Statement of the Problem	1
1.1.1 The U.S. Japan Cooperative Research Program and the 1/5 Scale Test Structure	1
1.1.2 Instrumentation of the Structure	2
1.1.3 Internal Force Transducers (IFT)	4
1.2 Objectives	6
1.3 Scope	7
2. FEASIBILITY STUDIES AND SELECTION OF THE LOCATION OF THE IFTs IN THE 1/5 SCALE TEST STRUCTURE, AND THEIR DESIGN AND FABRICATION	9
2.1 Feasibility Studies and Selection of the Location of the IFTs in the 1/5 Scale Test Structure	9
2.2 Design of the Column Internal Force Transducer	13
2.2.1 Column Characteristics	13
2.2.2 Development of Physical Characteristics of the IFT	17
2.2.3 Material for the IFT	20
2.2.4 Strain Gage Schemes for the IFT	22
2.3 Fabrication	24
2.3.1 Fabrication of the IFT Body	24
2.3.2 Strain Gaging Procedure	25

Page

3. CALIBRATION OF THE IFT 27

3.1 Calibration Methods 27

3.2 Evaluation of Calibration Methods 32

3.2.1 Evaluation of the Calibration Constants 32

3.2.2 Evaluation of Cross-Channel Interference 36

4. INSTALLATION OF THE IFT IN THE 1/5 SCALE STRUCTURE AND OBSERVED RESPONSES 39

4.1 Installation Procedure 39

4.2 Results of IFT Installations 41

4.2.1 Determination of Column Gravity Load 41

4.2.2 IFT Instability (Zero Drift) 45

4.3 Investigation of IFT Instability (Zero Drift) 46

4.3.1 Investigative Procedures and Methods 46

4.3.1.1 Monitoring of Installed IFTs 47

4.3.1.2 Drift Experiments Performed on IFTs 48

4.3.1.3 Drift Experiments Performed on Strain Gages Applied to 6061 Aluminum Test Specimens . 51

4.3.2 Results and Conclusions of the Investigation of IFT Instability (Drift) . . 56

4.4 Response of the IFT to Short Term Load Applied to the 1/5 Scale Structure 58

4.5 Response of the IFT to Long Term Sustained Loading of the 1/5 Scale Structure 60

Page

5. CONCLUSIONS AND RECOMMENDATIONS 65

REFERENCES 69

TABLES 71

FIGURES 77

LIST OF TABLES

Table		Page
2.1	Column Section Stiffnesses	71
2.2	IFT Load Ranges	71
2.3	IFT Material Mechanical Characteristics	71
2.4	IFT Section Stiffnesses	72
3.1	Calibration Constants for IFTS	73
3.2	Calculated Strain from Shunt Resistors	73
3.3	Measured Electronic Calibration	74
3.4	Statistical Analysis of Calibrations	75
3.5	Maximum Values of Cross Channel Interference . .	75
4.1	Maximum Upward Displacement of the Top of the Columns during the Installation of the IFTS	76
4.2	Summary of IFT Axial Force Channel Drift . . .	76

LIST OF FIGURES

Figure		Page
1.1	Plan of 1/5 Scale Model	79
1.2	Longitudinal Elevation of 1/5 Scale Model	80
1.3	Transverse Section of 1/5 Scale Model	81
2.1	Cross-Section of Model Columns	82
2.2	Longitudinal Section of Model Columns	82
2.3	Maximum First Story Column Loads for the 1/5 Scale Model	82
2.4	Internal Force Transducer Installation	83
2.5	Modified Cross-Section of the I.F.T.	84
2.6	Vertical Section of the Original Design Showing the Screwed Connection between the I.F.T. and End Plates	84
2.7	Sample of I.F.T. Plate Material Used to Test the Mechanical Characteristics of the 6061 Aluminum after Heat Treatment	85
2.8	Specimens Used to Determine the Weld Strength	85
2.9	Information on Gaging of Internal Force Transducer	86
2.10	Plan of the I.F.T. End Plate	87
2.11	Section A-A of the I.F.T. Showing the Section Modification and Welds	87
2.12	Section B-B of the I.F.T.	88
2.13	Section C-C of the I.F.T.	88
3.1	Original Device Used for Calibration of the I.F.T. Moment Channel	89
3.2	Typical Calibration Plot for an I.F.T. Moment Channel Using the Device in Fig. 3.1	89
3.3	Improved Device Used for Calibration of the I.F.T. Moment Channel	89

Figure		Page
3.4	Typical Calibration Plot for an I.F.T. Moment Channel Using the Device Shown in Fig. 3.3 . . .	89
3.5	Device Used for Combined Moment-Shear Calibration of the I.F.T.	90
3.6	Typical Calibration Plot for Combined Moment-Shear Loading of an I.F.T.	90
3.7	Set-Up Used for Axial Calibration of an I.F.T. .	90
3.8	The Effect of End Plate Restraint on the I.F.T. Strain Field under Axial Loading	90
4.1	Longitudinal Column Section Showing Steel Tube in I.F.T. Location during Construction	91
4.2	Measured Column Loads after Installation of all I.F.T.s	92
4.3	Measured Column Load after Each Individual I.F.T. Was Installed	92
4.4	Calculated Gravity Loads from Tributary Areas . .	92
4.5	Estimated Lower Bound for Column Forces Prior to I.F.T. Installation	92
4.6	Drift of 8 I.F.T. Axial Force Channels over 6 Weeks	93
4.7	Detail of Drift of the Axial Force Channel of I.F.T. #10	93
4.8	Example of Data Acquired from I.F.T.s during the Flexibility Tests. These Force Values Were Obtained during Loading of the 7th Floor of the Structure without Ballast	94
4.9	Distribution of Ballast Load from Transducer Readings and Concrete Strain Gages	94
4.10	Estimated Distribution of Ballast Load Accounting for Transducer Drift	94
4.11	Calculated Distribution of Ballast Load from the Actual Distribution of Ballast on the Structure	95
4.12	Tributary Areas Used by Chowdhury	95
4.13	Distribution of All Static Load from I.F.T.s . .	95
4.14	Calculated Distribution of All Static Load . . .	95

1 INTRODUCTION

1.1 Statement Of Problem

1.1.1 The U.S.-Japan Cooperative Research Program and the 1/5 Scale Test Structure.

This report is based on research which is part of the U.S. - Japan Cooperative Research Program Utilizing Large-Scale Testing Facilities. [1] The initial phase of this program, in the field of earthquake engineering, is devoted to the investigation of the performance of a seven-story frame-wall reinforced concrete (R/C) structure. It includes pseudo-dynamic testing of this structure at the Large-Size Structures Laboratory in Tsukuba, Japan. It also includes scale model shaking table experiments, to be performed at the Universities of: California, Berkeley; Illinois, Urbana-Champaign; and Stanford, California. Subassemblages of the structure are to be studied experimentally under pseudo-static loading conditions at Berkeley, the Universities of Stanford, California, and of Austin, Texas, and at the Laboratory of the P.C.A., Skokie, Illinois. This report is concerned only with the experimental studies to be conducted on a 1/5 scale model using the Earthquake Simulator (shaking table) facilities at the University of California, Berkeley.

The 1/5 scale model of the seven-story frame-wall structure, shown in Figs. 1-1, 1-2, and 1-3, will be subjected to a base motion in the direction of the longitudinal axis of the structure, as shown in Figs. 1-1 and 1-2.

The model was designed and constructed to maintain geometric similitude with the full-scale structure ; however, to fulfill mass similitude requirements, it is necessary to add auxiliary mass (ballast). This ballast is secured to the floor slabs so that it closely approximates the effect of gravity loads on the floor beams and columns without significantly altering the stiffness of the floor system.

To acquire sufficient information to study the response of this model to applied base excitations it is necessary to properly instrument the model.

1.1.2 Instrumentation of the Structure.

The response history of the total structure, as well as its main components will be measured using accelerometers, linear potentionmeter displacement transducers , and other deformation measuring devices. At least two accelerometers and linear potentiometer displacement transducers will be located at each floor level. From this the overall response (lateral force-displacement relationships) of the central longitudinal frame, containing the shear wall, and of

the external longitudinal frames can be obtained. Additional instruments will be located at the roof level, to measure the relative vertical displacements between columns.

Direct current differential transformers (DCDTS) will be used to measure local distortions, such as the fixed end and inelastic rotations of the end regions of beams and columns, and the flexural and shear distortion of the shear wall. At critical regions, local strains will be measured by strain gages applied to steel reinforcement. Concrete strain gages will be placed on the peripheral walls at the ends of the structure.

In wall-frame structures of this type, it is of considerable importance to evaluate the effectiveness of the shear wall, with respect to the frame, in resisting the lateral inertial forces due to the base motion. This can be accomplished by determining the distribution of base shear force between the columns and the shear wall. However, in statically indeterminate R/C structures, measuring force distributions of this type is extremely difficult. It would be possible to apply strain gages (or other distortion measuring devices) on the structural elements involved (in this case, the columns and the shear wall) to determine the internal forces. However, this is unreliable in the inelastic range, especially in the case

of concrete strain gages after some reversals of inelastic straining. Failure of a device could render the structure indeterminate. A more reliable method of measuring these force distributions is through the use of "internal force transducers," as described below.

1.1.3 Internal Force Transducers.

Internal force transducers (IFT) can be defined as devices capable of directly measuring the internal forces of a structural element. A simple IFT is a device which can be inserted in the structural member to measure internal forces. The advantages of this type of IFT are that the device can be:

1) Constructed from materials which have reliable force-deformation relations,
2) Reliably instrumented, and,
3) Properly calibrated so that it is possible to directly measure the internal forces.

The disadvantage is the potential for interference of the measuring device with the continuity of the structural elements in which the internal forces are being measured, i.e., the disturbance of the structural response that can be caused by the introduction of the IFT. However, with proper choice of location of the IFT and of its design criteria, this disadvantage can be overcome.

To eliminate or minimize discontinuity of the structural elements, the IFT design criteria should include careful selection of its different significant stiffnesses, and of the type of connection to the structural elements. Furthermore, according to the expected response of the element to which it will be connected, IFT design criteria should include careful consideration of the required sensitivity and range (capacity).

The IFT stiffness properties must be designed to match those of the element into which it is placed to minimize the disturbance of the response of that element. The IFT must be designed to withstand forces somewhat larger than the expected internal forces in the structural element without affecting its calibration. Thus the IFT must be designed so that the forces to which it is subjected (load range) will strain the IFT material within its elastic range only. Since the IFT instrumentation will measure strain of the IFT material, the sensitivity of the IFT output is directly affected by IFT stiffness. Therefore, this instrumentation should be chosen and located on the IFT so that its resolution corresponds (through a stiffness relationship) to small values of internal force.

The IFT material should be chosen so that the stress-strain relationship is linear within the load range. Linearity greatly simplifies the calibration procedures.

The installation procedure should be simple and should minimize disturbance of the structure. Finally, if several force quantities (bending moments shear, and axial forces) are being measured, each should be independent of the others.

In spite of the difficulties involved in designing, constructing and installing an IFT, it is believed that the advantages justify a detailed study to overcome these difficulties. Therefore, it was decided to make a detailed study of the possibility of using IFTs in the 1/5 scale model of the seven-story frame-wall R/C structure to be studied at Berkeley. This detailed study, reported herein, has the following main objectives.

1.2 Objectives

1. To study the feasibility of using internal force transducers (IFT) to determine the force distribution in the first story of the 1/5 scale model.
2. To develop design criteria for the IFT.
3. To design and fabricate the IFT.
4. To calibrate the IFT.
5. To develop installation methods and install and monitor the IFT in the 1/5 scale model.
6. To evaluate the response of the installed IFTs during tests conducted on the 1/5 scale model.
7. To formulate suggestions for further studies (according to experience and information gained in the above objectives) for improving design

criteria, fabrication, calibration and installation methods of these IFTs.

1.3 Scope

To accomplish the above objectives, the first step was to study the feasibility of using IFTs. When the results of this study were positive, general design criteria were established and the IFT location was selected. From this location specific design criteria were generated and a prototype was designed and fabricated. Preliminary studies on this prototype led to modifications and a final design.

The final design was fabricated in sufficient quantities for application in the 1/5 scale model. Calibration methods were developed using the prototype IFT and the production IFTs fabricated for the model. Each production IFT has been calibrated and calibration curves have been prepared to read internal forces (bending moments, shear and axial forces) independently.

After preliminary studies with one of the fabricated IFTs, 10 IFTs were installed in the model and their behavior was monitored over time and under the different loading conditions that were applied to the model. During the monitoring of their behavior, "zero drifts" were observed in some IFTs. A detailed study of this problem was conducted and is discussed herein.

Recommendations for further studies of the observed problems are formulated based on the data and experience gained from this study.

2 FEASIBILITY STUDIES AND SELECTION OF THE LOCATION OF THE IFTs IN THE 1/5 SCALE TEST STRUCTURE, AND THEIR DESIGN AND FABRICATION

2.1 Feasibility Studies and Selection of the Location of the IFTs in the 1/5 Scale Test Structure

In the experimental study of the 1/5 scale model of the seven-story frame-wall R/C structure subjected to base motion, it would be ideal to be able to determine the distribution of the total story shear between the shear wall and the columns at each story. Although this might be possible, it would involve both technical and economic difficulties.

Analytical studies show that for structures of this type, most of the inelastic behavior in the shear wall and the columns is concentrated in the first story. Studies demonstrate that it is feasible to instrument this critical story to determine the force distribution. Therefore, the first story columns were chosen as the most desirable element in which to place IFTs.

The precise location of the IFT was selected to be slightly above mid-story height of each first-story column. (Figs. 1-2, and 1-3) This location is the result of several considerations; most important among these were:

1) That the magnitude and distribution of the total base shear is of considerable interest in wall-frame structures of this type subjected to base motion,

2) That distribution of overturning moment at the base is also of great importance, and,

3) That to avoid significant interference with the flexural stiffness of the column, the ideal location is in the region of the column which typically has the lowest flexural demand.

Due to the above considerations, the IFT has been designed to independently measure the bending moment, shear, and axial force in the columns, near the mid-story height. (Figs. 1-2 and 1-3)

In determining the base shear distribution it is assumed that this distribution is the same at both the mid-story height of the first story, and at the foundation level. This implicitly assumes that the first story mass of the columns and shear wall have very small contributions to this base shear.

The inertial forces developed during the base excitation can be determined from the acceleration history of each floor level, if a lumped mass assumption is made. The external damping is typically quite small, with modal damping ratios (ξ_n) less than 2 percent. The ratio between the maximum modal damping force and the maximum modal inertial force is at most twice the model damping ratio, or less than 4 percent. Neglecting damping forces, and setting the restoring forces equal to the inertial forces will result in insignificant errors in the determination of the restoring forces. Therefore, the total base shear, which is the sum of the restoring forces, can be taken as the sum of the

inertial forces.

$$\underline{F}_I + \underline{F}_D + \underline{F}_R = 0$$

$$\underline{F}_I \doteq \underline{F}_R$$

$$V_B \doteq \sum_{n=1}^{7} F_{In}$$

The column IFT measures the shear carried by the columns. The remaining shear force must be carried by the shear wall (neglecting the contribution of the peripheral walls). Therefore, the distribution of base shear between the columns and the shear wall can be determined.

The total overturning moment resulting from the base excitation can be determined by a procedure which is similar to that used for determining the total base shear. This overturning moment is carried by the structure through flexure of the shear wall and axial force in the columns and the peripheral walls.

The axial force in the columns is measured by the column IFT. If a reasonable method for estimating the axial force in the peripheral end walls (from the force in the end columns or from concrete strain gages placed on the walls) is used, the overturning moment carried by the combination of the columns and the end walls can be estimated. The remaining moment must be carried by flexure of the shear wall. Therefore, the distribution of overturning moment can be determined.

An important criterion in the use of IFTs is the minimization of disturbance to the structural response by the indroduction of the IFT. The location of the

IFT in a region of low flexural demand in the first story columns is an attempt to minimize the effect of the IFT on the flexural stiffness of the columns. This flexural stiffness is an important factor in the distribution of base shear. The foundation (at the base of the column) is considerably stiffer than the beam-slab system (at the top of the column), leading to the conclusion that under most earthquake loading conditions a point of inflection is likely to be located slightly above the mid-height of the column.

Since axial force in the columns is measured by the IFT, the installation of the IFT into the column can be used to determine the distribution of gravity forces in the structure. A necessary assumption is that the installation of the IFT does not disturb the structure. (i.e., cause a lengthening or shortening of the element in which it is installed).

As previously discussed, it is necessary to add auxiliary mass to the 1/5 scale model to maintain mass similitude. It is also necessary to know the total axial stress level in the first story due to both gravity loads and the auxiliary mass. The distribution of load due to the auxiliary mass can be determined from the IFT, so that the total axial force in the columns prior to base excitation is known.

2.2 Design of the Column Internal Force Transducer

2.2.1 Column Characteristics

The design of an internal force transducer requires consideration of the characteristics of the structural member in which it is placed, as discussed previously (Sec. 1.1.3). In the case of the column IFT, a careful consideration of the characteristics of the first story columns should be made.

The typical first story column is a square section of reinforced concrete with eight longitudinal reinforcing bars, hoop type lateral reinforcement with cross ties. (Figs. 2-1 and 2-2) Each column is $3\frac{15}{16}$ in. (100 mm) square with an area of 15.5 in^2 (10,000 mm^2). Dimensions and typical spacing of reinforcement are tabulated with Fig. 2-1.

The ideal internal force transducer would be designed to have the same local stiffness properties as the part of the structural member which it replaces. However, this is impossible in practice, since reinforced concrete will have load dependent stiffness characteristics, while the structural metal used in the IFT will not exhibit these characteristics for the load range that it will be designed for. In addition, it is difficult to simultaneously match flexural, shear and axial stiffness. As a result, it is necessary to rate the relative importance of each stiffness type and to consider various load levels or limit states in determining stiffness.

Since the IFT is assumed to be located at or near a point of inflection in the column, the flexual demand should be low. Therefore, the flexural stiffness of the IFT is not very significant, although it should approximate the column stiffness to avoid the introduction of a large discontinuity.

In frame analysis it is common to neglect the shear deformations of beams or columns under lateral loads. If the length of the IFT is not large in comparison to the column, and the shear stiffness per length of the IFT is not very different from the shear stiffness per length of the column, the change in shear stiffness of the whole column caused by the introduction of the IFT will be small and insignificant. The change in the column's total lateral stiffness will be even less significant because the columns have been designed so that they will be subjected to relatively low shear.

The axial stiffness of the column is a major factor in determining the distribution of resistance to overturning moment. If the effect of the introduction of the IFT is to be minimized, the axial stiffness of the IFT must match that of the column part it replaces.

In summary, it is believed that in designing an IFT for columns in this type of structural system, the axial stiffness is most important, flexural stiffness less important, and shear stiffness least important.

In reinforced concrete structures, the intensity of axial stress, which depends on the load level (or limit

state) under consideration, has a considerable effect on member stiffness. Therefore, the comparison of IFT stiffness with the column stiffness must include consideration of the various significant load levels (limit states) which the columns are likely to experience.

Calculations of the column section stiffness have been performed assuming an uncracked elastic section [3]. Further calculations and other arguments [3] show that for flexure and shear the uncracked condition is the most important limit state occurring under the expected loading conditions at the IFT locations. Furthermore, the maximum expected level of axial stress is considered to be well within the elastic range of the concrete. The conclusion is that the uncracked elastic limit state is the only one which need be considered in calculating the column stiffness at the IFT location. The resulting column stiffnesses (stiffness per unit length) are given in Table 2-1.

In designing the IFT, the range of loads to which it might be subjected is an important criteria. An inelastic analysis was conducted for the full-scale seven-story frame-wall R/C structure. [4] Maximum column forces from the analysis were scaled appropriately to obtain the maximum expected first-story column loads in the 1/5 scale model. These are given in Figs. 2-3A and 2-3B.

To have some margin of safety in the use of the IFT, a factor of safety was considered for each of these maximum expected column loads (moment, shear, and axial force) to determine the IFT load range. The maximum bending moment along the length of the first-story columns will occur as an end moment due to the nature of the structural system and applied loads. If this maximum moment is taken as the design moment at the IFT location, no factor of safety is required since the moment at the IFT location can reach this maximum only in the highly improbable case of single curvature with maximum expected moments applied to each end. Since the maximum expected moment was 28.34 kip-inches, the design moment was taken as 30 kip-inches.

The maximum expected shear force in the first story columns is 1.62 kips. This maximum force will occur throughout the length of the column. Since there is some uncertainty in both the expected load and the shear capacity of the column and the IFT, a factor of safety of 1.4 was chosen and the IFT design shear force was taken as 2.3 kips.

The maximum expected axial compressive force in the first story columns is 11.32 kips. This maximum expected force will also occur throughout the length of the column. The columns may also be subjected to possible axial force overloads during any transport of the model, loading of the ballast, installation of the IFT or any other preparatory work, or due to differential

shrinkage between wall and column sections. Because of the uncertainty in the magnitude of these axial forces a safety factor of 1.4 was applied to the maximum expected axial compressive force to obtain a design load of 16 kips. It was not expected that the IFT would be subjected to axial tension during testing of the 1/5 scale model. However, the IFT should be expected to respond equally well to a tensile load of 16 kips.

The IFT load range is summarized in Table 2.2. These loads are the range of loads for which the IFT has to be calibrated and under which the IFT must exhibit strict linear behavior.

2.2.2 Development of Physical Characteristics of the IFT

The IFT consists of a short section of tube welded to two plates, one on each end of the tube. These plates are bolted to two additional plates which are welded to the column reinforcing steel (Fig. 2-4). The tube was constructed from a standard 4 in. O.D. extruded tube with a wall thickness of 5/8 in.. To insure uniformity of the cross section and a smooth surface for the application of strain gages, approximately 1/16 in. of material was removed from the inside and outside surfaces.

In the preliminary design, the IFT was to measure biaxial moments and shears, so a tube was selected, because of its identical properties along any two perpendicular directions. Due to fabrication difficulties and other problems, the biaxial scheme was dropped and the IFT was designed to measure bending moments and shear force in one plane only.

The length of the tube was limited to minimize the IFT's effect on structural response. However, to decrease the effect of the IFT's boundary conditions on the force measurements

obtained from the IFT instrumentation, it is desirable to have a minimum length to width (l/d) ratio of untiy. Therefore, the tube length is 4 in..

For thin walled tube sections, the shear stiffness is often taken as the product of the shear modulus (G) and the cross sectional area (A), with no modification factor for the area. The axial stiffness is taken as the product of the elastic modulus (E) and (A). Since E and G are of the same order of magnitude, the two stiffnesses will have values of the same order of magnitude. Therefore, if the applied shear and axial forces are of the same order of magnitude, the average shear strain and axial strain will have the same order of magnitude. However, in the column IFT the axial force will reach a larger magnitude than the shear force (Sec. 2.2.1, and Table 2-2). Axial strains will, therefore, be much larger than average shear strains, and if there is any cross channel interference (strain interaction), the ability of the shear channel to accurately measure small values of shear force can be impaired.

Tests of the prototype IFT showed that cross channel interference adversely affected the accuracy of the shear channel with shear strains corresponding to 0.35 kips of shear force being measured under 10.0 kips of applied axial force with no applied shear force. Although the amount of strain interaction was relatively small and the corresponding shear force is only 3.5% of the axial force, this 0.35 kips of shear force is a significant percentage (15%) of the design load for shear (2.3 kips). Increasing the sensitivity of the shear channel, without increasing the sensitivity of the axial force channel would reduce

the magnitude of shear force corresponding to the strain caused by interaction. However, increasing the sensitivity was difficult since the shear strain was already being measured near the neutral axial where it reaches its maximum value (per unit shear force).

The solution to this problem was to modify the cross section, reducing the tube wall thickness at the neutral axis to increase the maximum value of shear strain. This increased the shear sensitivity without removing too much of the total cross-sectional area. The modified cross section is shown in Fig. 2-5.

The plates to which the tube is welded are 3/4 in. thick by 5-1/2 in. square. They are designed to be relatively rigid, compared with the tube, to uniformly distribute the column loads from the bolted connection with the column to the IFT tube.

Originally, the tube was connected to each plate by 12 screws and the use of an inset for positive shear transfer (Fig. 2-6). However, this screwed connection was discarded in favor of welding since welding provides a better distribution of strain than screws, and because the screwed connection was suspected to be the cause of a hysteretic moment response in calibration (Sec. 3.1). The welded connection is more durable and reliable than the screwed connection over the lifetime of the IFT, especially if the IFT is applied in other future test structures.

2.2.3 Material for the IFT

The IFT is made from high strength aluminum because of its low elastic modulus and high yield strength. Because of availability and its easily reproduced temper, which gives a nominal yield strength of 40 ksi [5], 6061 aluminum with a T-6 temper was used.

In force transducers it is common to use 2024 aluminum with a T-3511 temper (nominal yield strength of 44 ksi [5]). This tempering procedure (T-3511) includes coldworking (straightening and stretching of the tube) to achieve high strength. The use of welding in this design requires annealing to remove residual stresses. Because of annealing, retempering is needed to return the required high strength. However, to avoid introducing new residual stresses or damaging the fabricated IFT, coldworking the annealed material was not considered to be desirable. Since the T-3511 temper could not be reapplied in full, it was believed that another type or aluminum should be selected so that the original tempering process could be easily reapplied to the fabricated IFT.

The alternative choice to the 2024 aluminum was the 6061 Aluminum with the T-6 temper. This tempering requires only heat treatment, which was accomplished easily after the welding and annealing. Samples of the material were obtained for testing of strength and stiffness (Fig. 2-7). Results of these tests are shown in Table 2-3.

The results of the tests of the aluminum samples give an average yield strength of 40.8 ksi, and an

elastic modulus of 10.2 x 10^3 ksi. These results are as expected, showing that the heat treatment was carried out according to specifications.

It should be noted that the high strength obtained (40.8 ksi), is not required to meet the IFT stress demands, but is desirable to insure linearity in the design load range (the maximum compressive stress expected considering the column load range is 12 ksi).

From the known material mechanical characteristics, the stiffnesses of the IFT were calculated. The calculated values are in Table 2-4 [3]. Comparison of Tables 2-1 and 2-4 shows that the stiffnesses of the tube compare reasonably well with the uncracked column stiffnesses. However, the stiffness of the entire assembly is somewhat larger (70.9 k vs. 59.1 ± 8.4 k for axial stiffness) due to the added stiffness of the plates. The stiffnesses of the assembly are given in Table 2-4.

As discussed previously, the tube is welded to the end plate. To determine if the weld strength is sufficient test coupons were provided by the fabricator (Fig. 2-8).

Tests on three coupons showed that they failed at an average tensile stress of 15 ksi. This failure was ductile and was centered at the center of the weld. The nominal strength for this weld (welding rod material is 4043 aluminum) after the T-6 tempering, is 40 ksi. [5] Therefore, the unexpected results of these tests show that something was wrong with these welds. The tests of the

6061 aluminum gave the expected results,indicating that the tempering process was applied correctly. It is believed that the unexpected results of the weld coupon tests are due to poor design of these coupon welds, and that these welds are not indicative of the welds on the IFT.

Figure 2-8 shows the weld test coupons. It is believed that the weld material was not as stiff as the rest of the material (i.e., a slightly lower elastic modulus) resulting in stress concentrations at the weld center. The weld center was observed to be a weak spot due to a lack of full weld penetration, and failure resulted.

In the IFT, the maximum value of tensile stress at the weld is expected to be less than 10 ksi, so a strength as low as 15 ksi would still be sufficient.

2.2.4 Strain Gage Schemes for the IFT

The strains developed on the IFT body during loading are measured using polyimide backed foil strain gages [3,6]. As previously discussed, three separate channels are used to measure moment, shear, and axial force. Each channel is comprised of an independent full wheatstone bridge of either four or eight strain gages. It is expected that the bridges, when wired correctly, will be temperature compensating and independent of each other (assuming an ideal strain distribution in the IFT body).

Strain gage locations and schematic wiring diagrams for each bridge are given in Fig. 2-9.

The general principle of a full wheatstone bridge is that strains (or change in resistance) of opposite arms are added, while strains of adjacent arms, are subtracted. When properly applied, this principle has the advantage of providing a simple way for temperature compensation, and also a way for increasing sensitivity.

For the moment bridge, gages on the same side of the IFT body are on opposite arms (hence they are added) while gages on opposite sides of the IFT are on adjacent arms (hence they are subtracted one from the other). The result of this is that for bending, positive strains are added and negative strains are subtracted (thus adding their absolute value). The output of the bridge is then four times the extreme fiber strain. For pure axial force, or thermal strain, added and subtracted values have the same magnitude and sign, so the bridge output is zero.

The shear bridge is similar to the moment bridge. In the shear bridge, gages with the same orientation are added (by being on opposite arms), gages with different orientations are subtracted one from the other (by being on adjacent arms). For applied shear, gages with opposite orientation will experience strains of opposite signs and their absolute values will be added. In this case the bridge output will be four times the shear strain. For axial load, or thermal strain, gages with opposite orientation experience strains of the same sign and

magnitude, and subtraction yields no net strain.

The axial bridge has longitudinal gages on opposite arms with lateral gages on arms adjacent to the longitudinal gages. As a result, under axial load the longitudinal strains are added and the lateral strains (which are of opposite sign due to poisson's effect) are subtracted. This gives a bridge output of 2.6 times the actual longitudinal strain, (for poisson's ratio of .3). For thermal strain, lateral and longitudinal strains are of equal sign and magnitude, so subtraction yields no net strain. Bending strains are cancelled because gages of symmetric location with respect to the axis of bending are on the same arm of the bridge. This addition of strains yields no net strain for pure bending.

2.3 Fabrication

2.3.1 Fabrication of the IFT Body

The final design was fabricated according to the drawings in Figs. 2-10, 2-11, 2-12, 2-13. The specifications are given in Reference 3.

Procedures and tolerances for fabrication are detailed in the specifications. As the first step in this fabrication, the tube was cut to proper length and 1/16 in. of material was removed from the inside and outside surfaces, as shown in Fig. 2-12. Then the

plates were cut to size and the insets (Fig. 2-10 and 2-12) were machined in the plates. The plates and tube were aligned and welded, and the entire assembly was heat treated. Then the cross-section modification was made, with flat surfaces being machined for location of the shear strain gages. Finally the top and bottom surfaces of the plates (the end surfaces) were machined to insure that they were parallel, and to provide good bearing surfaces. The basic tolerence was ±.005 in..

2.3.2 Strain Gaging Procedure

The procedure for application of the strain gages is similar to that outlined in the directions which are enclosed in packages of Micro-Measurements M-Bond 610. [6] Strain gages, adhesive, and coatings were obtained from a commercial manufacturer. Details of these products are in Reference 3.

The major variation from the procedure described in Reference 6 is in surface preparation. For these transducers, sandblasting with a fine abrasive is used instead of abrading with fine sandpaper and using a mild etching solution, as suggested. The neutralizer for the etching solution also was not used. This modifed procedure is common practice in the laboratories at Davis Hall, University of California, Berkeley.

After wiring the circuits, a polyurethane coating [3], is applied for moisture protection. A thin

sheet metal cover was fabricated and wrapped around each IFT tube to physically protect the strain gages.

3 CALIBRATION OF THE IFT

3.1 Calibration Methods

In the application of force transducers, it is necessary to relate the strain output of the wheatstone bridge to an applied load through some type of calibration function (or calibration constant, for linear calibration functions). In this way, the applied load can be determined from the bridge output measured. This calibration function can be determined analytically or experimentally. For most applications, it is convenient if this is a linear calibration function.

To determine a calibration function analytically, the constitutive relationship of the transducer material and the cross-sectional properties are needed. The procedure is to determine the stress due to a unit load, at appropriate gage locations, from the section properties, and then apply the constitutive relation to determine the strain. The strains for the appropriate gages are then combined in the same manner as the bridge combines them to obtain bridge output. Reference 3 contains calculations for calibration functions for the IFT used in this study. The calibration function is linear due to an assumed linear constitutive relationship. Only the value of the linear constant is needed to define the function. The constants for each of the channels are in Table 3-1.

The experimental determination of the calibration constants is more important, because it yields more dependable values than analytical methods. However, in experimental methods it is very important to be certain of the boundary conditions (support conditions, points of load application, and dimensions) so that the magnitude and distribution of the internal forces applied to the transducer are accurately known. If these forces are properly known, it is a simple matter to determine the relationships between them and the measured strains.

The procedure used for the determination of a calibration constant for the moment channel is a good example of the importance of boundary conditions. Figure 3-1 shows the device used initially for moment channel calibration. The IFT is installed at the center of a "beam". This beam is composed of sections of 2 in. nominal diameter steel pipe ($I=.666\ in^4$) with plates welded on each end. One set of plates is used to bolt to the IFT, the others extend down to a reaction table, forming the supports for the beam. Simple support conditions are assumed. Point loads are applied equidistant from the ends (Fig. 3-1) providing constant bending at the IFT location. The known load is applied using a Baldwin-Southwark electro-hydraulic 60 kip test machine.

Typical results of this moment calibration are shown in Fig. 3-2. Note the hysteretic response, mentioned in Sec. 2.2.2, which is caused by frictional forces developed at the load points and supports, i.e. where the end plates are supported on the reaction table of the testing machine. These frictional forces have moment arms about the centroid of the beam. They restrain the beam ends, decreasing moment at the IFT during loading, and increasing the moment at the IFT during unloading.

An improved calibration beam is shown in Fig. 3-3. The reactions are located at the centroid and are free to rotate. Therefore, the simple support assumption is justified. Loads are applied with rollers that can rotate through small angles. The tube sections that compose the beam are 4 in. square steel tube ($I=10.7$ in^4). This is much stiffer than the pipe used initially, consequently decreasing the deflections of the beam, improving the response.

Typical results of this calibration are shown in Fig. 3-4. Since the calibration procedure involves measuring the strain due to an applied force, the calibrations are plotted with strain at the ordinate and force as the abcissa. The units of the calibration constants

are, therefore, $\frac{\mu in/in}{unit}$ of force. Moment calibration constants are given in Table 3-1.

The calibration of the shear channel is accomplished through a procedure similar to moment calibration. A single load is applied to the beam device described above (Fig. 3-5). The support conditions are different than those for constant moment loading. In this case, one support is located at the centroid at the end of the beam. The other support is located closer to the IFT, with the reaction being provided by a roller applied to the 4 in. tube. The beam is assumed to be simply supported. Both moment and shear channels are monitored in this calibration. To complete the calibration of the moment and shear channels, the beam is turned over so that the IFT is loaded from the opposite direction.

Typical results of this calibration are shown in Fig. 3-6. Shear calibration constants are in Table 3-1.

The calibration of the axial force channel is a simple procedure although careful consideration of the boundary conditions is again required. Since the IFT has a l/d ratio of unity, it is important to distribute the load to the IFT end plates in a uniform manner. The reaction table on the

test machine has a rough surface from years of use. To provide uniform bearing, several smooth plates are stacked between the table and the IFT, and between the IFT and the load head. Also, a universal joint, free to rotate in all directions, is used in providing the load (Fig. 3-7).

For the axial calibration, as well as the other calibrations, it is necessary to load the IFT above the specified load range before calibration to insure a stable zero reference. This "overloading" is effective in relieving residual stresses in the strain gages due to their application. For all the calibrations 4 to 6 cycles of loading were used, until the strain reading corresponding to zero load remained constant for 2 load cycles. Data for calibration was then taken in one load cycle. Axial load calibration constants are in Table 3-1.

To verify proper calibration of any data acquisition system to which the IFT is connected, it is necessary to be able to apply a known "force" to the IFT, even though it may be installed in the test structure. This is accomplished by inserting what is commonly called a "shunt" resistor into the wheatstone bridge circuit. This resistor is connected parallel to one arm of the bridge, inducing a change in the resistance of that arm of the bridge. This corresponds

to an apparent change in strain, or an apparent applied load, which can be read by the data acquisition system. Calculated values of "applied load" for a given shunt resistor can be compared with the values measured by the data acquisition system. This insures proper calibration of the data acquisition system.

This procedure is called electronic calibration. Values of the apparent load induced by the shunt resistors have been measured with a Budd Box strain indicator. These values have also been calculated in Reference 3. Calculated values are in Table 3-2 and measured values in Table 3-3. These values can be used to check the calibration of any data aquisition system used with the IFT.

3.2 Evaluation of Calibration Results

3.2.1 Evaluation of the Calibration Constants

From Table 3-1, it is obvious that there is a significant difference between calculated calibration constants and the values obtained through experimental calibration. In general these differences can be attributed to a difference between the specified cross section and the actual cross section, and the phenomena of "strain averaging", which is the result of using large strain gage lengths in regions of varying strain, so that the measured strain is smaller than the maximum strain in that region.

Table 3-4 has the results of a brief statistical study of the calibration constants. From the small magnitude

(1.2%) of the coefficient of variation (COV) of the experimentally determined moment calibration constants, it is apparent that the moment of inertia (I) is reasonably constant for all twelve IFTs, (since $\epsilon = \frac{Mc}{I} E$ and E can be assumed to be constant). However, it appears that the actual I is larger than calculated from the specified cross section, (since the experimental calibration constants are smaller than calculated). Part of the difference between the calculated and the mean experimental values may be due to an averaging of strain by the strain gages. Figure 2-9 shows that only an edge of each gage is at the location of extreme fiber strain. The rest of the gage is under smaller values of strain, since it is located closer to the neutral axis as a result of the surface curvature.

The experimentally determined shear calibration constants have a large COV (15.4%). This is probably due to differences in the tube wall thickness among IFTS at the shear gage location, since shear strain is very sensitive to thickness ($\tau = \frac{VQ}{tI}$). The original tube thickness was reduced during fabrication of the IFT to increase the sensitivity of the shear channel. (Sec. 2.2.2) However, in fabrication (Sec. 2.3.1) this modification of the wall thickness was made after welding of the plates. This made it difficult for the machinist to stay within the desired

tolerance; therefore each IFT may have a slightly different modified wall thickness.

From Figs. 2-5 and 2-13, it can be seen that the wall thickness at the location of the shear gages becomes larger with distance from the neutral axis. Also, the value of Q (from $\tau = \frac{VQ}{tI}$) becomes smaller at larger distances from the neutral axis. Therefore, in the IFT shear strain decreases rapidly with distance from the neutral axis. The calculated shear calibration constant is determined for a location at the neutral axis. However, the shear gages have finite length and cover an area located away from the neutral axis. Therefore, these gages will be under an average strain which is less than the strain value at the neutral axis. This, in addition to the possibility of a thicker wall due to machining error, is the reason for the 36.4% reduction from the calculated calibration constant.

The experimentally determined axial calibration constants have a very small COV (1.8%). This is because the cross-sectional area (A) is nearly constant for all twelve IFTs ($\epsilon=\frac{P}{AE}$). Note that neither the area (A), nor the moment of inertia (I), is sensitive to errors in the wall thickness at the neutral axis (since the elementary area at the neutral axis has a small contribution to A and I).

The mean axial calibration constant is 35.4% less than the calculated constant. This is probably due to a larger than specified cross-sectional area and differences between assumed strain fields and actual strain fields. The differences between the actual and specified cross sections have already been discussed. In general the actual cross section is somewhat larger.

A more significant reason for the difference between experimental and calculated axial calibration constants is the constraining effect of the end plates, which causes the strain field to be different than assumed. When the IFT is compressed axially, the tube will expand radially if unrestrained. But, the plates on the end restrain the tangential strain (measured by lateral gages) throughout the length of the IFT. They also cause a "bulging" of the IFT tube, creating tensile bending stresses on the exterior surface of the tube, when the tube is compressed (Fig. 3-8). These bending stresses decrease the compressive strain measured at the surface of the IFT. The restraint of the plates was not considered in the calculated constant.

In general, the calibration results are linear and repeatable. It has been found that they can be reproduced with less than 0.5% error, with additional loading cycles.

This repeatability is important in transducer use. Although there are differences between calculated and experimental calibration constants, the reasons given for the differences are plausible, and the obtained experimental calibration constants should give sufficient sensitivity.

3.2.2 Evaluation of Cross-Channel Interference

Cross-channel interference is the measurement of strain in channels which are not expected to measure strain under the given loads. (These channels will be referred to as "unloaded" channels. "Loaded" channels are channels which should measure strain under the given loads.) An example would be the axial and shear strain readings obtained during the constant moment calibration under pure bending moment. During all calibrations both loaded and unloaded channels were monitored. Table 3-5 has approximate values of the range of maximum loads obtained in the unloaded channels. The mean values (Table 3-5) are the averages of maximum loads obtained from unloaded channels from the 12 IFTs.

The values in Table 3-5 show that there may be some interference between channels, expecially when one type of force has a relatively large value. However, most of

this interference is believed to be due to errors in the methods of load application during calibration, which will not occur in the test structure.

In the constant moment calibration, the axial and shear channels always read negative values. The axial force is probably due to local compression from the nearby application of point loads. Shear force is probably a result of error in the location of the point loads. In the axial load calibration, the moment and shear forces are probably due to an eccentric loading. Interference of this type can occur when the IFTs are installed in the structure, if there is an eccentricity between the column segments, to which the IFT is attached. It is believed that eccentricities of this type will be minimal in the structure. Other sources of interference, such as gage misallignment, uneven distribution of stress from the plates through the weld to the tube, or from strain discontinuities, can also occur after the installation. However, interference from these sources is not expected to be significant.

4 INSTALLATION OF THE IFT IN THE 1/5 SCALE STRUCTURE AND OBSERVED RESPONSES

The calibrated IFTs were installed in the test structure and used to measure column forces under several static loading conditions. "Zero drifts" were observed and an extensive investigation of the zero drifts was undertaken. The results of this investigation and the observed response of the IFT to several loading conditions of the model, as well as details of the installation, are presented in this chapter.

4.1 Installation Procedure

The ideal installation would be to install the IFT before casting the concrete during construction of the model. However, the IFTs were not finished prior to construction, and the IFT location was filled by a 4-1/2 in. O.D. steel tube. Four bolts prestressed the two installation plates to the tube to insure a continuous moment and shear connection (Fig. 4-1). The procedure for replacing this tube with the IFT is detailed in this section.

First, ten IFTs (one for each column excluding the shear wall edge members), are connected to a low speed scanner, data acquisition system. Proper calibration constants are input into the system, so that the strain output of each wheatstone bridge of the IFT can be converted into force values. Therefore, the output of the system will be force quantities.

Initial strain readings are measured and stored by the data aquisition system. These correspond to zero force in all channels. Future strain readings will be compared with these initial values, and the change in strain will be converted to force values by the system.

Next, each IFT is installed individually. First, the prestress in the steel tube is released and the upper installation plate is raised using the four installation bolts (threaded rods shown in Fig. 4-1). The steel tube is removed, the upper plate is lowered back to its original position, and the installation plate surfaces are cleaned for IFT installation. Dial gages are used to measure how far the top of the column is raised, and to insure that the upper installation plate can be returned to its original position. Table 4-1 gives the maximum displacement of the top of the column during this procedure. It should be noted that column A3 was inadvertently left in the displaced position after removing the steel tube.

Next, the IFT is positioned. The bolts to connect it to the steel plates are placed loosely and shims are installed in the spaces left for hydrostone (see Fig. 2-4). Initially, four shims are placed in the space between the lower set of plates, one shim from each side.

Then, four shims are pushed into the spaces between the upper set of plates. These shims are pushed in from each side until approximately 1 kip of axial force is measured. The shims are then adjusted so minimum values of shear force and moment are measured.

Next, the spaces are filled with hydrostone, which should insure an even distribution of further forces. After the hydrostone has dried, the four outer bolts which were used to raise the upper plates, and which had supported the column load, are removed. The bolts connecting the IFT end plates to the installation plates are tightened and the IFT supports all of the column load. The installation of all ten IFTs takes several days.

4.2 Results of IFT Installations

4.2.1 Determination of Column Gravity Load

It was expected that the installation of the IFTs in the columns of the 1/5 scale model would allow the determination of the gravity load carried by the columns. However, the installation took several days, and during this time a severe "zero drift" of the axial force channels occurred.

This "zero drift" can be described as a change over time of the measured output strain of the IFT, without any

change in the load being applied. Since the data acquisition system reads strain relative to an initial value of strain (corresponding to zero load) this measured change in strain is read as an apparent load. The measured values of axial force in the columns at the end of the installation of all the IFTs are given in Fig. 4-2. It is obvious that these unrealistic values are primarily the result of drift.

To get a reasonable determination of the actual gravity forces in the columns, it was necessary to find the difference between each IFT's output prior to installation and immediately after. These values are given in Fig. 4-3, and can be compared with values obtained from analysis [2] in Fig. 4-4.

From Fig. 4-3, it can be seen that the sum of the column loads obtained from the IFT installations is larger than the weight of the structure [2]. Equilibrium requires that the total load in the four peripheral walls and the shear wall be tensile. The actual distribution of this tension is unknown.

There are two causes for this unexpected distribution of gravity force. The major cause is the different rates of concrete shrinkage between the walls and the columns. The columns are 100 mm (3 15/16 in) square. The main shear

wall panel is 40 mm (1 37/64 in) thick x 900 mm (35 14/32 in) wide, and the peripheral walls are 30 mm (1 3/16 in) thick x 800 mm (31 1/2 in) wide. These dimensions indicate that the concrete in the walls would tend to shrink faster initially than in the columns. In the case of the peripheral walls (due to the proximity of the peripheral walls to the nearby columns) the columns offer considerable restraint and consequently differential shrinkage could relieve all the compressive force from gravity and induce large tensile force in the walls, while inducing additional compressive force in the nearby columns. The effects of differential shrinkage are magnified because the IFT location does not shrink, since there is no concrete there. Shrinkage in the main shear wall panel is unlikely to induce significant compression in any of the columns because of the small restraint offered by the columns as a consequence of the relatively large distance to the nearest columns. However, the panel itself is likely to be under tension with the shear wall edge members under increased compression.

Analytical studies of this differential shrinkage [8] show that it is capable of inducing up to 10.6 kips of compression in columns A1, A4, C1, and C4, and 12.8 kips of compression in columns B1 and B4. In this case each peripheral wall would be under 17.0 kips of tension. A comparison of Figs. 4-3 and 4-4 shows that columns A1,

A4, C1, and C4 are on the average under 3.2 kips more compression than expected, while columns B1 and B4 are on the average under 3.3 kips more compression than expected. These forces are well below those which differential shrinkage is capable of inducing.

The other cause of this unexpected distribution of gravity force is the disturbance to the structure by the IFT installation procedure. This procedure did not insure that the final relative distance between the installation plates was the same as the initial distance. During removal of the steel tube, the displacement of the top of the column was controlled to within $\pm$ 5x10^{-5}in. This insured that the distance between the plates, after removal of the tube was within $\pm$ 5x10^{-5}in. of the initial distance. During the rest of the installation procedure, this distance was not as well controlled. The effect of altering the distance between the installation plates is that the structure above the IFT location is subjected to support settlements or uplifts.

Calculations have been performed to determine a lower bound for axial compression in the columns prior to IFT installation [3]. Results of these calculations are in Fig. 4-5. Comparison of Figs. 4-3 and 4-5

shows that the IFT installation caused some disturbance to the structure. In column A3, the disturbance was significant (since the top of the column was inadvertently left .0032 in. too high after removal of the steel tube), with about 46% of the axial compression in this column potentially due to the IFT installation. For the other columns, the effect of the IFT installation was less significant, with a maximum of 14%, (in columns C2 and C4) and an average of 10% of the axial force in these columns potentially due to the IFT installation.

It should be noted that for all the columns, except one (C 1), the net effect of the IFT installation was equivalent to a support uplift. The combination of this uplift, and differential concrete shrinkage is the source of the relatively high compressive forces in the columns.

4.2.2 IFT Instability (Zero Drift)

The problem of IFT instability or zero drift has been mentioned briefly in Sec. 4.2.1. This problem was first noticed in the axial force channels, but subsequently drift was also observed in the shear force channels. No drift was observed in the moment channels. Initially, in the axial force channels, drift was in the positive direction (tension) for nine of the ten installed IFTs. IFT #11, in column C2, had negative drift (several months later, negative drift was observed in two other axial force channels).

The drift in the shear channels varied with both positive and negative drifting observed.

The total drift of the axial channels over three months is given in Table 4-2. Figure 4-6 shows a plot of the variation with time of the force output of eight of the ten axial channels under a "constant" load. This load corresponds to the column loads determined from the installation procedure. However, as previously discussed, a substantial part of these loads was due to differential shrinkage between the walls and the columns. It is expected that this part of the column loads would be reduced with time as column shrinkage increased relative to wall shrinkage. This reduction of compression would contribute to the positive force values (tension) indicated by the IFTs. But, the large magnitude of the total forces indicated by the IFTs (Fig. 4-6) leads to the conclusion that there are other more significant contributing factors. Therefore, a detailed investigation of the cause of this zero drift was carried out.

4.3 Investigation of IFT Instability (Zero Drift)

4.3.1 Investigative Procedures and Methods

The investigation of the IFT zero drift problem was accomplished in several ways.

1) IFTs in the test model were closely monitored.
2) Experiments were performed on uninstalled IFTs (12 IFTs were fabricated and 10 were needed in the test model).
3) Experiments were performed on strain gages applied to

bars fabricated from the IFT end plate material.

4) Direct telephone consultation was made with engineers who had extensive experience in the application of commercially manufactured strain gages.

4.3.1.1 Monitoring of Installed IFTs

The IFTs which were installed in the test model were closely monitored during the three months following installation. Output was recorded so that it was possible to follow the drift of the IFTs over time. Figure 4-6 is a plot of the output (in force units) of 8 of the 10 axial channels over a 6 week period. Table 4-2 summarizes three months' of data for the axial force channels. Figure 4-7 is a detailed plot of axial force data from IFT #10 in column C1. From this plot, it can be seen that the force output has an overall drift, and also varies during each day.

The variation during the day is the result of a thermal cycle experienced by the structure each day. The IFT is aluminum and has a higher coefficient of thermal expansion than the rest of the structure (reinforced concrete). It is, therefore, expected that the columns should have an increase in compressive force (Fig. 4-7) as the structure warms up each day. Because of this variation, the data plotted in Fig. 4-6 is all from the same time of day, 8:00 a.m.

It was not possible to find any explanation of this type for the overall drift. The pattern of drift was more random in nature, and the magnitude of the force output was too large to have any structural justification. It is believed that environmental factors were affecting the IFTs, not through thermo-mechanical behavior of the structural material, but by some type of interaction with the strain gages themselves, the strain gage adhesive, or the strain gage coating. Further investigations were conducted in this direction.

The IFTs have been monitored again, most recently at the time of this writing (nearly five months after installation), and the drift has continued to this date. The rate has slowed significantly, with typical values of less than 0.5 kip drift per week in the most active axial force channels. The shear force channels also continue to drift as before, while the moment channels remain stable.

4.3.1.2 Drift Experiments Performed on IFTs

It was initially believed that the drift observed might be due to a failure of the strain gage adhesive under long term loading. To test this, IFT #9 (which had been installed in column C4 and exhibited severe drift in its axial force channel) was removed from the 1/5 scale model and its axial force channel was recalibrated. The calibration results

were within 0.5% of the original calibration. IFT #9 was also placed in a creep test machine designed for concrete cylinders. It was loaded with 30 kips for 3 weeks under constant temperature conditions (73.3°F). No significant change in the output of the axial force channel was observed. It was then concluded that the drift was not a direct result of mechanical loading of the IFT.

It had been previously observed that the IFTs had not exhibited drift during the time they had been in the laboratories in Davis Hall, where strain gage application, calibration, coating of the gages, etc., had been done. When they were moved to the location of the 1/5 scale model in the Earthquake Simulator Building at the Richmond Field Station, the drift problems began. Since Davis Hall has a reasonably constant environment (temperature and humidity) while the Earthquake Simulator Building does not, it was concluded that the drift problem was related to environmental factors.

The constant temperature rooms located in Davis Hall were used to simulate a severe temperature cycle that might occur in the Earthquake Simulator Building during a 24 hour perior. This cycle included:

1) 11 hours in a 40°F room, simulating typical night temperatures,
2) 2 hours in a 20°F room (with the IFT insulated so

that the temperature of the IFT was slightly below 40°F) simulating extreme night temperatures,

3) 3 hours in a 40°F room, and 4 hours in a 73.3°F room, simulating the warming up during the morning,

4) 1 hours in a 100°F room (again with the IFT insulated) for the warmest part of the day, and

5) finally 3 hours in a 73.3°F room.

IFT #5 was put through this temperature cycle on two occasions. The net drift for these two cycles was +43 $\mu in/in.$ and +50 $\mu in/in.$ in the axial force channel, (the other channels were not monitored). This corresponds to forces of 1.06 kip and 1.23 kip respectively. IFT #9 was put through this cycle and drifted 23 $\mu in/in.$ in the axial force channel (corresponding to a force of .56 kip). From these tests it was concluded that the cycling of temperature in the Earthquake Simulator Building was a contributing factor in the drift problem.

Consultation was made with other engineers experienced in the application of commercially manufactured strain gages. They believed that contaminants in the adhesive or underneath the coating could be activated by temperature cycles. It was suggested that one of the axial force bridges be unwired, so that the gages could be monitored independently to better identify the cause of drift.

The axial force channel of IFT #5 was unwired and each gage was monitored individually. It was observed that output of axially oriented strain gages was drifting in a positive direction at a faster rate than that of the laterally oriented gages, giving a net positive drift for the bridge. (Note, if they drifted at the same rate the bridge would subtract one from the other, leaving no net drift.) No particular gage could be identified as the source of the problem, rather most of the gages exhibited some positive drift in their output, with the rate of drift varying with time.

It was concluded that the cause of drift was not unique to any gage, but common to all gages in the drifting channels. Contaminants in the adhesive, or in the coating were believed to be the sourse of drift, and their rate of activity was being affected by temperature cycling.

4.3.1.3 Drift Experiments Performed on Strain Gages Applied to 6061 Aluminum Test Specimens

To identify the actual cause of the drift problem in the IFTs, additional strain gages were applied to two samples of the 6061 aluminum used in fabricating the IFT end plates. Three types of strain gages were used:

1) Gages of the type (from the same manufacturing lot) used in the axial force channel of the IFT's.

2) Gages of the type (from the same manufacturing lot) used in the moment channel on the IFT's.

3) New gages, which were similar to the moment channel gages in size and shape, but made with a different backing material [3].

These gages were applied to the specimens, following procedures used in fabricating the IFTs, but using extreme care in avoiding contamination of the adhesive. The gages were oriented and wired to form axial force bridges, with two axial gages and two lateral (poisson) gages. One bridge was made from IFT axial force channel type gages, one was made from IFT moment channel type gages, and two bridges were made from the new gages.

After application of the gages, the exposed surfaces of the gages were carefully cleaned of all contaminants. Then the specimens were subjected to low level ($10ksi \pm .25f_y$) tensile loading. After this the specimens were put through two thermal cycles, as described in the previous section. One bridge of each gage type was monitored as a whole, and one bridge of the new gages was unwired, so that its gages could be monitored independently. After each test, the exposed gage surfaces were cleaned to remove

any contaminants which might have collected there during the test.

As a result of these temperature cycles, no significant drift occurred in the output of any of the full bridges. The maximum change in the output of a full bridge was 7 $\mu in/in$, observed in the bridge composed of the new gages. The bridge composed of the IFT moment channel gages was absolutely stable, with no drift occurring. The maximum drift in the output of the individually monitored gages was observed to be 11 $\mu in/in$. This was fairly consistent among these gages, with the average drift being 10 $\mu in/in$ per gage per temperature cycle.

The cleaning of the exposed gage surfaces was observed to have a more considerable effect on the gage output than the temperature cycles. The maximum net drift in the output of a bridge due to the cleaning was 17 $\mu in/in$. Typical values ranged from 4 to 15 $\mu in/in$, but there was no observed drift in the bridge composed of IFT moment channel type gages. The maximum net drift in an individually monitored gage was 15 $\mu in/in$.

From these tests, it was concluded that the treatment of the exposed gage surface was critical, and that the drifts observed as a result of the temperature cycle of these gages were from activity on this gage surface, not from any activity in the strain gage adhesive. The IFT

moment channel gages are encapsulated gages [3], meaning that a thin film of electrically insulating material has been placed over the electrically conductive foil of the strain gage. The other gages are not encapsulated so the exposed surface of the gage is actually the surface of the electrically conductive foil. Therefore, it is obvious why the treatment of this surface is so important and why the IFT moment channel gages behaved so well during these experiments.

In light of this, new experiments were performed to determine how the preparation of the exposed surface of the un-encapsulated gages affects the output of the gage during temperature cycles. In the first of these tests three of the new gages were given different surface treatments. One was contaminated with dirt and oil typically found on human hands and coated with the polyurethane coating used on the IFTs. Another was carefully cleaned and coated with the same coating. The third gage was carefully cleaned and coated with an electrically insulating acrylic coating, followed by a coat of polysulfide modifed epoxy. This coating combination is considered to be suitable for general field applications.

The results of the application of an extended temperature cycle (lasting two days) to these gages indicated the following:

1) A drift of 48 $\mu in/in$ was observed in the output of the contaminated gage,
2) The output of the un-contaminated polyurethane coated gage drifted 4 $\mu in/in$, and
3) The output of the more heavily coated gage drifted 8 $\mu in/in$, but there is uncertainty in this value due to a suspected wiring problem.

The three gages were then subjected to a second temperature cycle (of the type described in the previous section) but the results were less conclusive. The heavily coated gage had no drift observed in its output, but small drifts were observed in the output of the polyurethane coated gages. The gage with contamination under the coating drifted 6 $\mu in/in$, and the gage without any contamination under the coating drifted 8 $\mu in/in$.

The bridge composed of IFT axial force gages was then unwired so that its gages could be read independently. One pair of gages was contaminated and coated with polyurethane. The other pair was carefully cleaned and coated with the heavier coating described above. These gages

were subjected to two 24 hour temperature cycles (of the type described in section 4.3.1.2).

The results of these tests showed that the more heavily coated un-contaminated gages had no drift in their output. The contaminated polyurethane coated gages showed significant drift in their output, with a maximum value of 20 $\mu in/in$ per cycle observed on one gage. An average value of 13 $\mu in/in$ of drift per cycle was observed in these gages.

It was concluded from these experiments that the treatment of the exposed surface of the un-encapsulated strain gages is very important in the performance of the strain gage, expecially if the temperature varies at the gage location. It was also concluded,that, for the gages applied to the 6061 aluminum specimens, the strain gage adhesive was not a factor in any observed drift.

4.3.2 Results and Conclusions of the Investigation of IFT Instability (Drift)

It was observed that the drift of the output of the shear and axial force channels has no relationship to load of any type, either short term or long term. The drift is unpredictable as far as specific magnitude over a given time is concerned. But, in general, the rate of drift has decreased over time. For short periods of time, the sign

or direction of drift can be predicted, although over long periods of time, a few weeks, this may change. There was no drift observed in the moment channels of the IFT.

A daily cycle of load in the axial force channels of the IFT was observed to correspond to the variation of temperature in the Earthquake Simulator Building. A large difference in the coefficient of thermal expansion between the IFT material and the model's structural material was the cause of this.

It is believed that contaminants acting on the top face of the strain gages in the shear and axial force channels (which are un-encapsulated or open faced gages) are the primary cause of the drift. These contaminants are underneath the polyurethane coating, and appear to be activated by the daily variation of temperature in the Earthquake Simulator Building.

The polyurethane coating may also be a contributing cause to the drift. The Earthquake Simulator Building was considered to be standard laboratory conditions for strain gages, but the variations of temperature and humidity justify the use of a thicker, more moisture-proof coating.

In conclusion, although the choice and application of strain gages is not a simple matter, some generalizations may be made.

1) Select encapsulated gages when possible. The IFT moment channel gages are such gages.
2) When using gages which are open-faced (un-encapsulated), coat the bottom and top surfaces with adhesive when applying [6]. An alternative would be to carefully clean the gage after application, and immediately apply a moisture-proof coating.
3) After soldering wires to the gages, carefully remove rosin flux and clean gage surface before applying final coatings.
4) The top surface of un-encapsulated strain gages requires as much attention as the bottom surface.

4.4 Response of the IFT to Short Term Load Applied to the 1/5 Scale Structure.

The response of the IFT to short term loading was observed during the flexibility tests conducted on the 1/5 scale structure [2]. In these tests the structure

was subjected to static lateral loads at the seven-floor heights (one floor at a time), and the lateral displacements of the floors were measured, giving flexibility coefficients.

The IFTs were used to obtain the loads in the first-story columns. Figure 4-8 gives the force values obtained during loading of the seventh floor, normalized for 1 kip of applied lateral load. The actual load applied was 5 kips, so the forces measured were five times the value given in Fig. 4-8.

The maximum actual measured values were:

0.580 kip-in bending moment

0.200 kip shear force, and

1.550 kip axial force.

Comparison of these values with the IFT load ranges (Table 2-2) shows that the column loads were relatively small and, therefore, more prone to error.

However, the IFT response does not appear to exhibit significant errors. The distribution of force is reasonably symmetric and the values make sense physically. Drift of the IFT channels was not a problem, due to the short length of time of the test.

The column shear forces measured were used to obtain the distribution of shear between the shear wall and the

columns as described in section 2.1 of this report. This was done for the application of loads to each of the seven floors. The results of these tests, and interpretation of these results are given in detail by Aktan, Bertero and Chowdhury. [2]

4.5 Response of the IFT to Long Term Sustained Loading of the 1/5 Scale Structure.

The need to add ballast to the 1/5 scale model was discussed in Sec. 1.1.1. The ballast was loaded onto the structure over a period of five days. It was desirable to determine the distribution of the additional gravity forces from the ballast, but due to the length of time required to load the ballast, it was expected that drift of the IFT axial force channels would make this determination difficult, or unreliable.

Figure 4- 9 gives the distribution of the ballast load as determined directly from IFT axial force channel output, and from the output of concrete strain gages applied to the peripheral walls. From study of the recent history of the IFT output, it was determined that the readings of certain axial force channels had been drifting significantly. The output of these four axial force channels (IFT #4 in column A2, IFT #12 in column A4, IFT #6 in column B1, and IFT #2 in column C3) was modified to give the estimated distribution of ballast load given in Fig. 4-10.

To perform this modification it was first necessary to determine the direction of drift, and the relative rate of drift. The axial force channels in columns A2, A4 were observed to be drifting at a relatively rapid rate. The axial force channels in columns A2, B1 were observed to be drifting in a negative direction while the axial force channels in columns A4, C3 were drifting in a positive direction. All other drifts were considered insignificant.

To modify the drifting channels, measurements of the column loads (from the IFTs) when the structure was partially loaded, were scaled appropriately to give column loads when the structure was fully loaded (eg. the loads when only two of seven floors were fully loaded were scaled by 7/2). It was thought that scaling loads measured earlier in time would contain less drift error. It was also necessary to use data acquired at the same time of day as that in Fig. 4-9 (late afternoon) due to the daily variation of column load discussed in Sec. 4.3.1.1.

From the actual distribution of ballast on the structure, the expected distribution of ballast gravity force was calculated and is given in Fig. 4-11 [8]. Comparison of Figs. 4-10 and 4-11 shows good agreement between the calculated results and the experimental results for the central columns of frames A and C, and the shear wall. However, the experimental

results show the peripheral walls are carrying more load, and the end frame columns are carrying less load than expected.

The reason for the difference between the experimental and calculated results is the tributary areas used by Chowdhury [8], to calculate the distribution of ballast gravity force. These tributary areas (Fig. 4-12) were used to analytically distribute ballast loads from the slab to the beams, without enough consideration of relative stiffnesses of these beams. The transverse spandrel beams on the ends of the structure are directly supported by the peripheral walls. The ballast load transferred to these beams is carried directly by these walls as axial forces. Ballast load which is transferred to the other beams is carried by flexure to the nearest column. It is obvious that the spandrel beams will be much stiffer than the other beams. Therefore, they will attract more ballast load than predicated from the tributary areas in Fig. 4-12. As a result the peripheral walls carry more ballast load, and the nearby columns carry less ballast load, than was calculated.

The total static axial forces were summed from experimental results (Fig. 4-13) and from calculated results (Fig. 4-14). The experimental results are incomplete due to the

unknown distribution of the shrinkage induced forces (Sec. 4.2.1)

The results given in this section show that it is possible, in certain cases, to use the IFT to measure the application of the load over time. However, it is necessary to consider the drift which can occur over the loading time and account for it appropriately, if possible.

For the case of ballast loading, accounting for drift was fairly simple. Since the structure was under service level conditions, an assumption of linear elastic behavior was justifiable. Also, the load was applied in constant increments (i.e., each floor had the same load), so it was possible to diminish the effect of drift with time by scaling the column loads obtained (earlier in time), when the structure was partially loaded. For other cases of long term sustained load, or in attempting to study redistribution of gravity loads within the structure, accounting for IFT drift may be much more difficult, or perhaps impossible.

5. CONCLUSIONS AND RECOMMENDATIONS

From the design studies conducted for an internal force transducer (IFT) for the 1/5 scale test structure, it was concluded that:

1) The choice of location of the IFT within the test structure is crucial, since proper location will minimize disturbance to structural response. Also, this location determines the specific requirements for IFT stiffness, sensitivity, load range, and connection type.

2) For measuring the internal forces of the first-story columns, the best location for the IFT was slightly above the mid-story height of the columns. For this region of typically low bending moment, the uncracked elastic condition was the only limit state required for consideration in determining IFT stiffness criteria, although the possibility for minor flexural cracking does exist.

3) For structures of this type, and for this IFT location, the axial stiffness of the IFT is most important, with flexural stiffness being less important and shear stiffness being least important.

4) All of the stiffnesses of the entire IFT assembly are larger than the uncracked elastic column stiffness due to the large stiffness of the connecting plates.

From study of the response of the prototype IFT and fabrication of the IFTs, it was concluded that:

1) The original shear sensitivity was too small, allowing for severe cross-channel interference from axial loads. Major modifications to the cross-section of the IFT were required to alleviate this.

2) In the instrumentation of IFTs the proper application of strain gages is crucial.

From the calibration and installation of the IFTs, it was concluded that:

1) The experimental calibration set-up should be simple with known boundary conditions to precisely determine the internal forces.

2) Installation procedures are important, since disturbance to the structure will have an effect on subsequent structural response.

3) The zero drift observed in the IFT output was due to the activity of contaminants on the top surface of the strain gages. The rate of activity was stimulated by temperature cycling.

4) The overall performance of the IFT was considered acceptable for short term static or dynamic loading.

To improve design and fabrication of future IFTs it is recommended that:

1) The stiffness of the entire IFT assembly, including

the IFT attachments, should match the stiffness of the structural element in which it is located.

2) Aspects of the IFT material in addition to the obvious strength and linear elastic requirements should be considered. The strength of the material selected should be unaffected by fabrication, or easily regained by heat treatment. The coefficient of thermal expansion of the IFT material should match that of the structural material to avoid undesirable thermal stresses.

3) The IFTs should be installed into the structure at the appropriate time during construction, or procedures for installation into completed structures should be improved to avoid unnecessary disturbance to the structure.

4) Studies of the effect of the IFT on the response of the 1/5 scale structure to dynamic loads should be conducted. The effect of the IFT on the distribution of forces within the structure should be studied analytically. Pseudo-static testing of structural subassemblages with and without the IFT should be conducted to study the effect of the IFT on column stiffness.

5) Further design studies be made to determine what parameters control the level of cross-channel interference in IFTs.

REFERENCES

1. "Recommendations for a U.S.-Japan Cooperative Research Program Utilizing Large-Scale Testing Facilities," U.S.-Japan Planning Group, Cooperative Research Program Utilizing Large-Scale Testing Facilities, UCB/EERC-79/26, September 1979.
2. Aktan, A.E., Bertero, V.V., and Chowdhury, A.A., "Experimental and Analytical, Static and Dynamic Responses of a 7-Story 1/5-Scale Model Frame-Wall Structure at Service Level," August 1982 (EERC In House Report To Be Published).
3. Sause, R., "A Transducer for Measuring the Internal Forces in the Columns of a Frame-Wall Reinforced Concrete Structure." Appendices, Unpublished SESM Research Report, University of California, Berkeley, December 1982.
4. Charney, F.A., and Bertero, V., "An Evaluation of the Design and Analytical Seismic Response of a Seven Story Reinforced Concrete Frame-Wall Structure," UCB/EERC-82/08, July 1982.
5. Welding Kaiser Aluminum, Knight, J.W., Ed., Kaiser Aluminum and Chemical Sales, Inc., Oakland, CA., 1967.
6. "Strain Gage Installations with M-Bond 43-B, 600, 610 Adhesive Systems," Micro Measurements Bulletin B-130-7. Measurements Group, Inc., Raleigh, N.C., 1977.

7. Harris, H.G., Bertero, V.V., and Clough, R.W., "One-Fifth Scale Model of a Seven Story R/C Frame-Wall Building under Earthquake Loading," Proceedings, International Seminar on Dynamic Modeling of Structures, Building Research Establishment, Garston, Watford, England, November 19-20, 1981.

8. Chowdhury, A.A., "Mechanical Charateristics (Static and Dynamic) of the Materials Used in, and of the Whole 1/5 Scale Model of the U.S.-Japan Seven-Story R/C Test Building," (Unpublished In House Research Report).

9. Nakata, S., Baba, A., and Ito, H., "Damage Aspects and Hysteresis Properties after Repair and Installation of Nonstructural Elements," Proceedings, The 3rd JTCC Meeting, Building Research Institute, Ministry of Construction, Japan, July 14-20, 1982.

TABLE 2-1 COLUMN SECTION STIFFNESSES

Flexural	Shear	Axial
$(79.0\pm11.3)\times10^{3}$kip-in^{2}	$(20.5\pm3.7)\times10^{3}$kip	$(59.1\pm8.4)\times10^{3}$kip

TABLE 2-2 IFT LOAD RANGES

Moment	Shear Force	Axial Force
± 30k-in	± 2.3kip	± 16.0 kip

TABLE 2-3 IFT MATERIAL MECHANICAL CHARACTERISTICS

Specimen	Yield	Ultimate	Elastic Modulus
Specimen A	39.20ksi	44.32ksi	10.3 $\times10^{3}$ksi
Specimen B	42.32ksi	44.08ksi	10.1 $\times10^{3}$ksi
Average	40.76ksi	44.20ksi	10.2 $\times10^{3}$ksi

TABLE 2-4 IFT SECTION STIFFNESSES

Section	Flexural	Shear	Axial
Original tube	99.1×10^3 k-in^2	25.3×10^3 kip	67.3×10^3 kip
Tube with 1/16" off surfaces	78.3×10^3 k-in^2	20.2×10^3 kip	53.8×10^3 kip
Modified X-Section	75.1×10^3 k-in^2	$15x7 \times 10^3$ kip	41.9×10^3 kip
IFT End Plates	216×10^3 k-in^2	50.8×10^3 kip	162×10^3 kip
Installation Plates	619×10^3 k-in^2	149×10^3 kip	464×10^3 kip
Equivalent for Entire Assembly	114×10^3 k-in^2	25.9×10^3 kip	70.9×10^3 kip

TABLE 3-1 CALIBRATION CONSTANTS FOR IFTS

	Moment	Shear	Axial
Calculated	103 $\frac{\mu in/in}{kip\text{-}in}$	740 $\frac{\mu in/in}{kip}$	63.6 $\frac{\mu in/in}{kip}$
Experimental * IFT #1	88.0 $\frac{\mu in/in}{kip\text{-}in}$	458.3 $\frac{\mu in/in}{kip}$	39.3 $\frac{\mu in/in}{kip}$
#2	89.2 "	492.3 "	42.6 "
#3	86.6 "	472.9 "	40.7 "
#4	86.6 "	463.4 "	40.1 "
#5	85.5 "	473.7 "	40.6 "
#6	86.4 "	468.9 "	41.3 "
#7	86.5 "	470.5 "	40.8 "
#8	86.3 "	465.8 "	41.6 "
#9	86.4 "	470.7 "	41.4 "
#10	87.1 "	475.1 "	41.9 "
#11	88.4 "	474.8 "	41.9 "
#12	86.3 "	459.8 "	40.8 "

* Experimental calibration constants for Moment and Shear are an average of calibration results from loading in both senses. Experimental calibration constants for axial force are an average of calibration results for compressive loading.

TABLE 3-2 CALCULATED STRAIN FROM SHUNT RESISTORS

Moment		Shear		Axial	
270 kΩ	18 kΩ	475 kΩ	47.5 kΩ	1000 kΩ	150 kΩ
221 μin/in	3266 μin/in	126 μin/in	1263 μin/in	120 μin/in	794 μin/in

TABLE 3-3 MEASURED ELECTRONIC CALIBRATION

IFT #	Moment Calibration					Shear Calibration					Axial Calibration				
	Mech. Cal. Const. μin/in kip-in	Shunt * Strain (μin/in)		Equivalent Force ** (kip-in.)		Mech. Cal. Const. μin/in kip-in	Shunt * Strain (μin/in)		Equivalent Force ** (kip)		Mech. Cal. Const. μin/in kip-in	Shunt * Strain (μin/in)		Equivalent Force ** (kip)	
		270kΩ	18kΩ	270kΩ	18kΩ		470kΩ	47kΩ	470kΩ	47kΩ		1000kΩ	150kΩ	1000kΩ	150kΩ
1	88.0	+222	+3272	2.52	37.18	458.3	+125	+1261	.273	2.751	39.3	+118	+790	3.00	20.1
2	89.2	+221	+3274	2.48	36.70	492.3	+126	+1259	.256	2.557	42.6	+121	+793	2.84	18.6
3	86.6					472.9					40.7				
4	86.6	+220	+3272	2.54	37.78	463.4	+128	+1261	.276	2.721	40.1	+120	+796	2.99	19.85
5	85.5	+219	+3273	2.56	38.28	473.7	+125	+1259	.264	2.658	40.6	+119	+794	2.93	19.6
6	86.4	+219	+3272	2.53	37.87	468.9	+126	+1259	.266	2.685	41.3	+119	+792	2.88	19.2
7	86.5	+220	+3273	2.54	37.84	470.5	+124	+1262	.264	2.682	40.8	+119	+796	2.92	19.5
8	86.3	+221	+3272	2.56	37.91	465.8	+125	+1262	.268	2.709	41.6	+120	+794	2.88	19.1
9	86.4	+221	+3273	2.56	37.88	470.7	+125	+1261	.266	2.679	41.4	+120	+796	2.90	19.2
10	87.1	+221	+3274	2.54	37.59	475.1	+125	+1262	.263	2.656	41.9	+121	+796	2.89	19.0
11	88.4	+219	+3271	2.48	37.00	474.8	+128	+1263	.270	2.660	41.9	+120	+795	2.86	19.0
12	86.3	+220	+3271	2.55	37.90	459.8	+127	+1262	.276	2.745	40.8	+120	+792	2.94	19.4

* Apparent strain read by strain indicator after application of shunt resistor

** Equivalent force value related to the shunt strain: $F_{shunt} = \frac{\epsilon_{shunt}}{C}$

TABLE 3-4 STATISTICAL ANALYSIS OF CALIBRATIONS

Channel	Calculated Constant	Mean Value for 12 IFT Constants	Standard Deviation	Coefficient of Variation	% Difference from Calc. Constant
Moment	103 $\frac{\mu in/in}{kip\text{-}in}$	86.9 $\frac{\mu in/in}{kip\text{-}in}$	1.1 $\frac{\mu in/in}{kip\text{-}in}$	1.2%	15.6%
Shear	740 $\frac{\mu in/in}{kip}$	470.5 $\frac{\mu in/in}{kip}$	8.9 $\frac{\mu in/in}{kip}$	15.4%	36.4%
Axial	63.6 $\frac{\mu in/in}{kip}$	41.1 $\frac{\mu in/in}{kip}$	.9 $\frac{\mu in/in}{kip}$	1.8%	35.4%

TABLE 3-5 MAXIMUM VALUES OF CROSS CHANNEL INTERFERENCE

Calibration Type	Channel, Range, Mean	Channel, Range, Mean
Constant Moment	Axial Force, -0.5 to -2.0k Mean = -1.0k	Shear Force, -0.2 to -0.5k Mean = -0.3k
Combined Moment-Shear	Axial Force, 0.0 to -0.5k Mean = -0.35k	--
Axial Load	Moment, -2.7 to +2.3 kip-in Mean = +0.7 kip-in	Shear Force, -0.1 to +0.2k Mean = +0.07k

TABLE 4-1 MAXIMUM UPWARD DISPLACEMENT OF THE TOP OF THE COLUMNS DURING THE INSTALLATION OF THE IFTS*

Column	A1	A2	A3	A4	B1	B4	C1	C2	C3	C4
IFT No.	#8	#4	#1	#12	#6	#7	#11	#10	#2	#9
Disp. (in.)	0.0020	0.0050	0.0032	0.0020	0.0041	0.0019	0.0060	0.0100	0.0095	0.0031

* All were lowered back to their original position $\pm 5 \times 10^{-4}$ in. except A3

TABLE 4-2 SUMMARY OF IFT AXIAL FORCE CHANNEL DRIFT

Column-IFT #	Drift Over Time Intervals (kip)					3 Month Total(kip)	μin/in Equivalent
	4/8-4/13	4/13-4/23	4/23-4/29	4/29-6/7	6/10-6/30		
A1 - #8	2.8	2.1	2.3	9.6	4.4	21.2	882
A2 - #4	3.6	0.3	-0.7	3.8	-9.8	-2.8	-112
A3 - #1	-1.2	-2.7	0.6	10.9	5.5	13.1	515
A4 - #12	0.9	1.1	0.8	11.7	10.6	25.1	1024
B1 - #6	-0.2	-0.5	1.0	2.9	-3.5	-0.3	-12
B4 - #7	2.5	-0.5	0.9	4.7	1.1	8.7	355
C1 - #10	-0.4	0.2	0.9	3.7	1.6	6.0	251
C2 - #11	-2.4	-1.3	-0.5	-6.9	-1.3	-12.4	-520
C3 - #2	5.4	3.3	1.5	10.5	6.2	26.9	1146
C4 - #9	0.7	4.9	-0.5				397
	#9 was changed to #3 5/3						
C4 - #3				1.0	-0.8	0.2	8

FIGURES

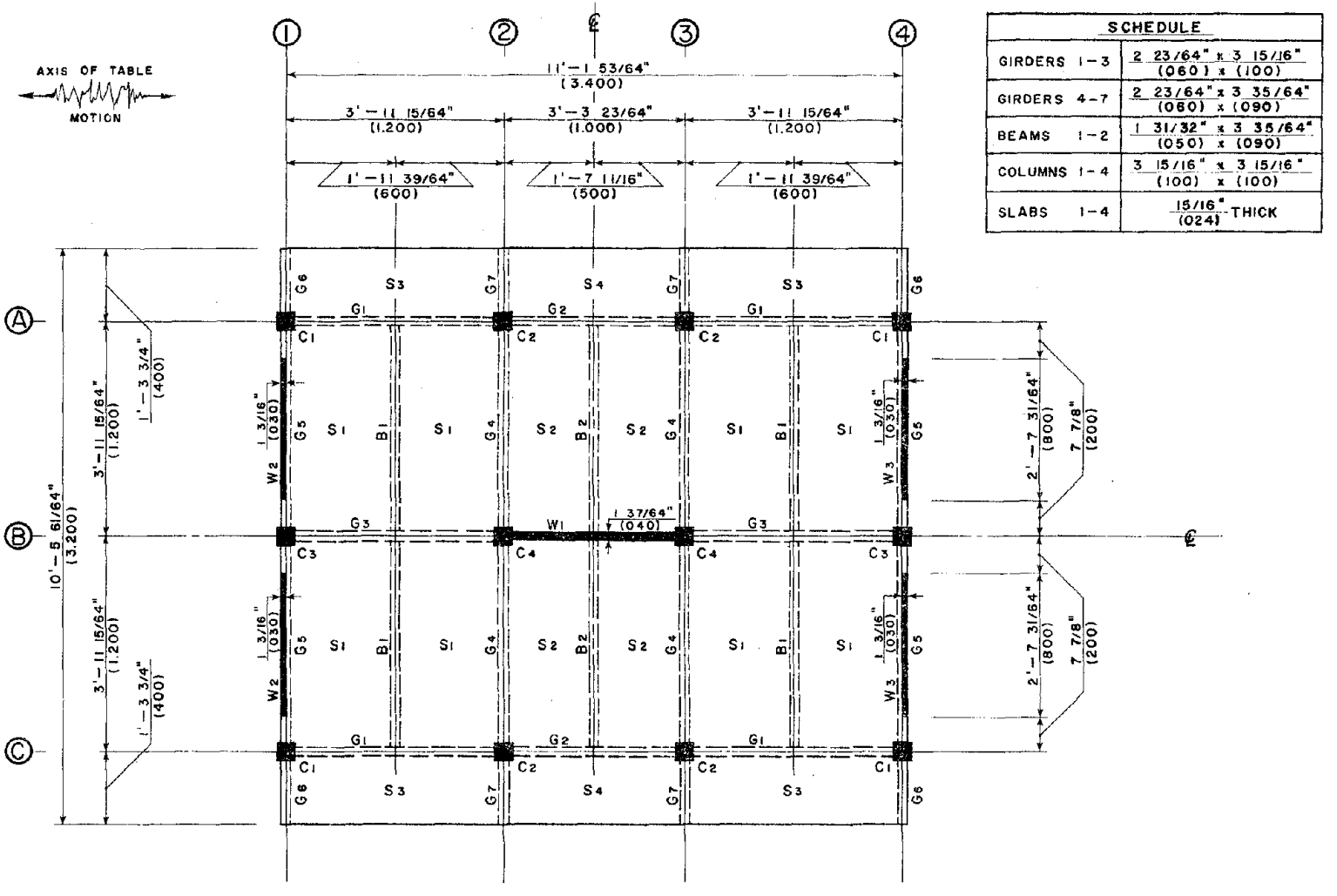

FIG. 1-1 PLAN OF 1/5 SCALE MODEL. (After Harris EtAl; [7])

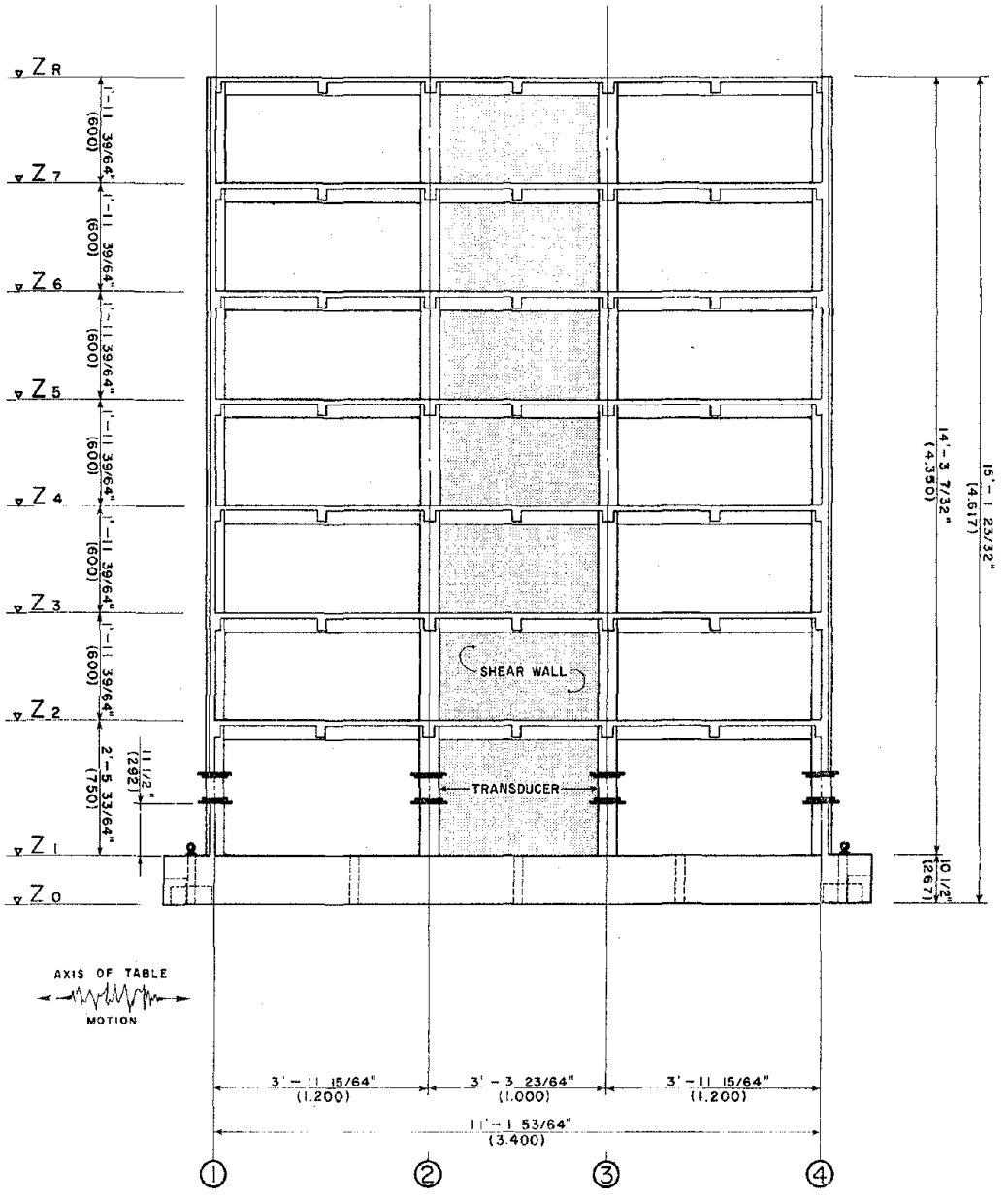

FIG. 1-2 LONGITUDINAL ELEVATION OF 1/5 SCALE MODEL.
(After Harris EtAl; [7])

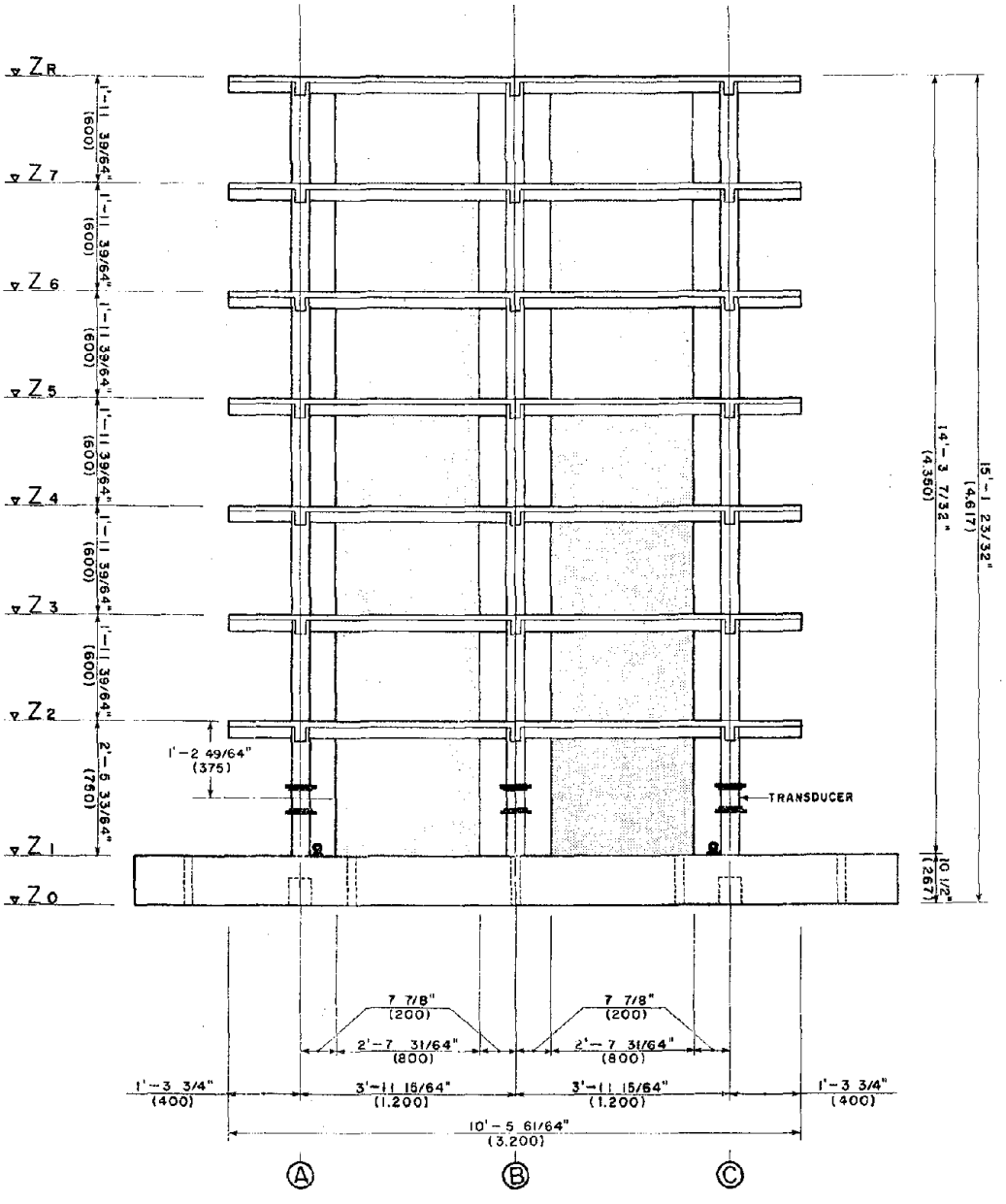

FIG. 1-3 TRANSVERSE SECTION OF 1/5 SCALE MODEL.
(After Harris EtAl; [7])

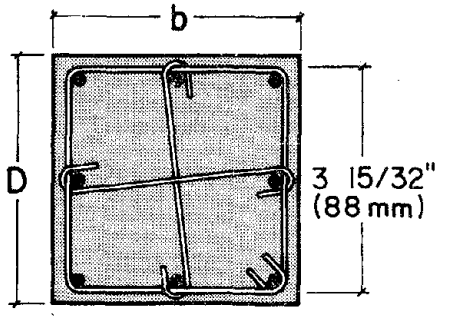

b x D = 3 15/16" x 3 15/16" (10 cm x 10 cm)	
PRINCIPAL REIN.	8 - D4.4 mm
HOOP D-2 SPACING O.C.	25/32" (20 mm)
CROSS TIE D-2 SPACING O.C.	VARIES

FIG. 2-1 CROSS-SECTION OF MODEL COLUMNS.

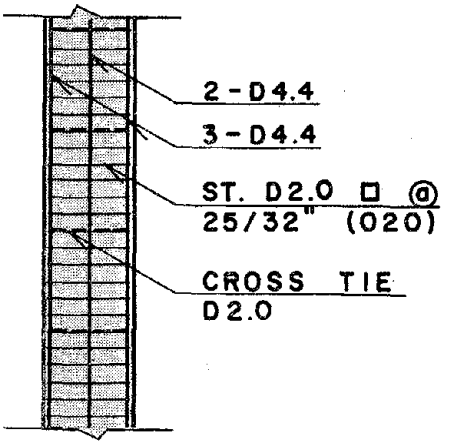

FIG. 2-2 LONGITUDINAL SECTION OF MODEL COLUMNS.

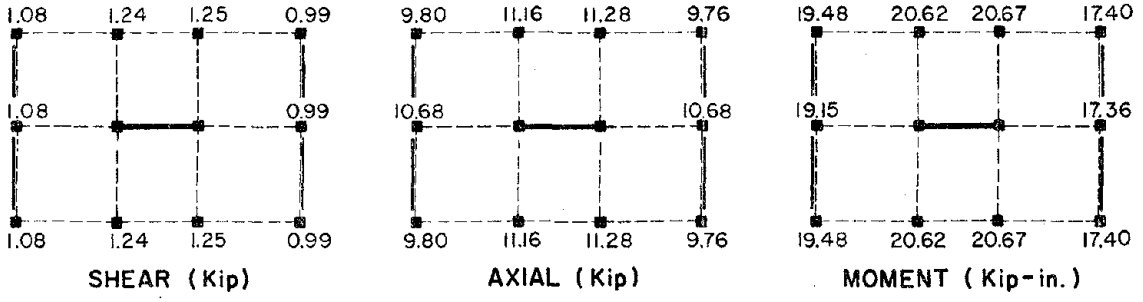

(a) ANALYSIS USING MIYAGI-OKI GROUND MOTION. [4]

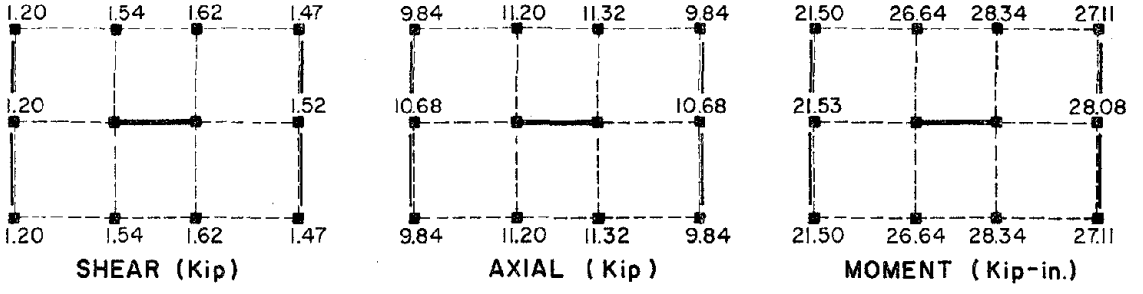

(b) ANALYSIS USING DERIVED PACOIMA DAM GROUND MOTION. [4]

FIG. 2-3 MAXIMUM FIRST STORY COLUMN LOADS FOR THE 1/5 SCALE MODEL.

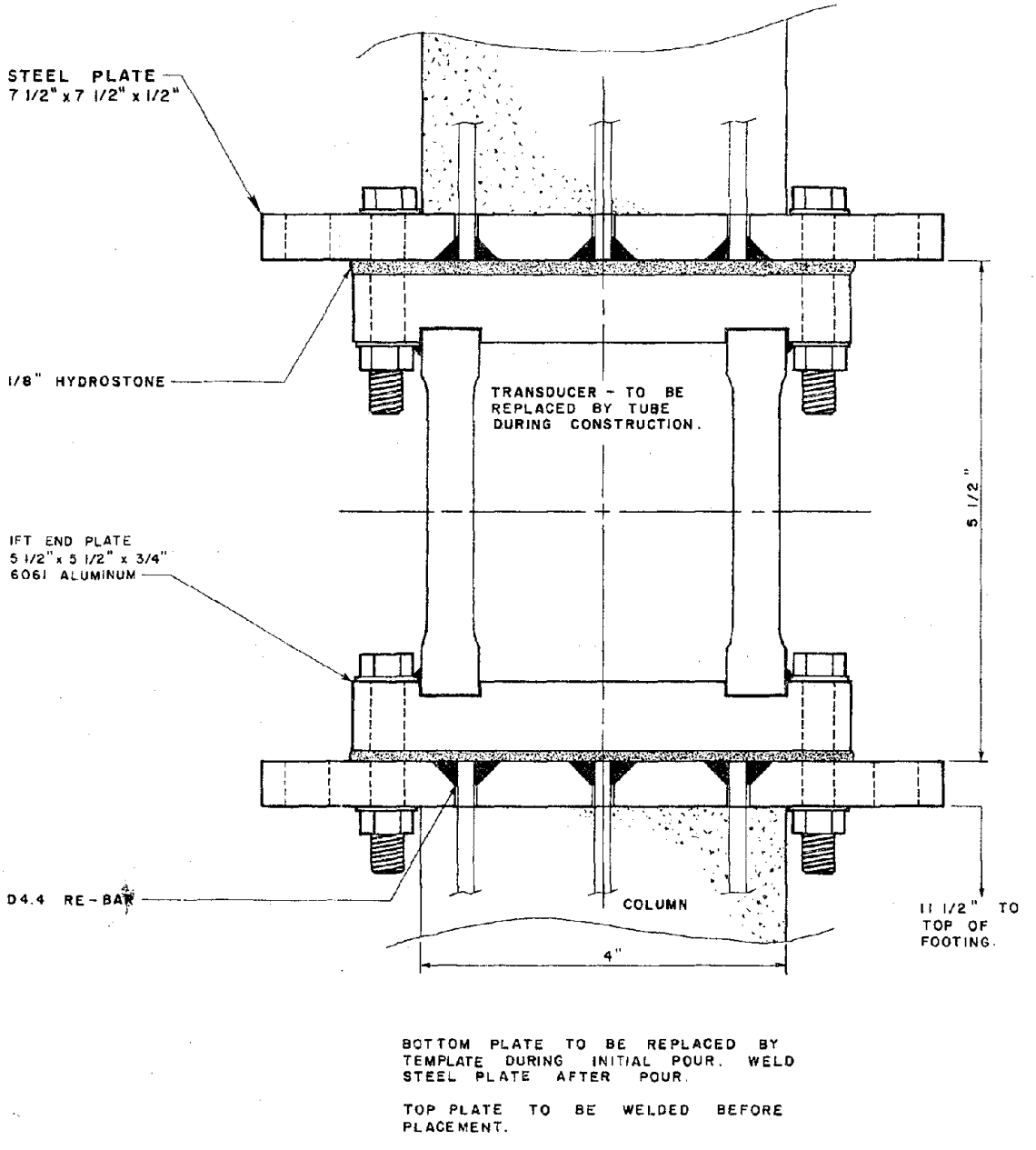

FIG. 2-4 INTERNAL FORCE TRANSDUCER INSTALLATION.

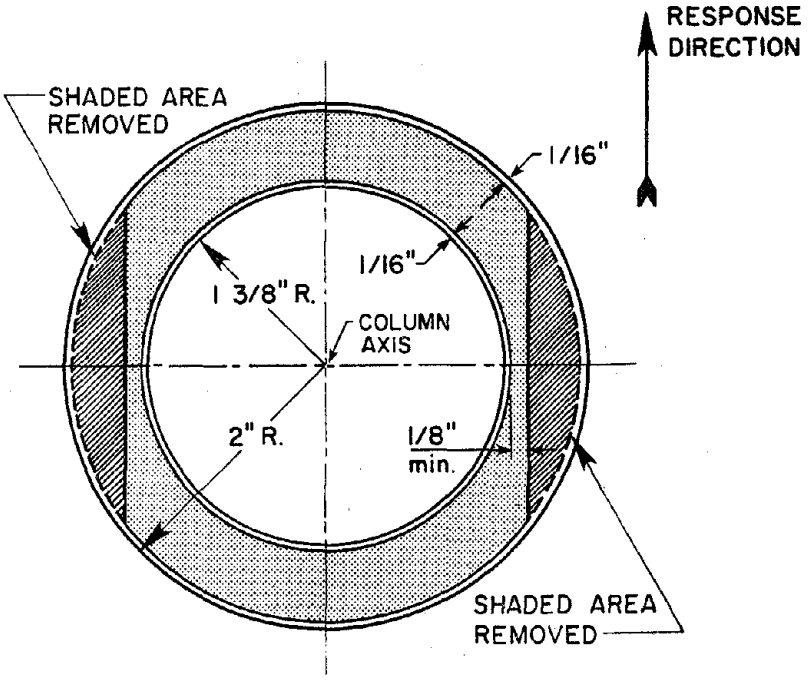

FIG. 2-5 MODIFIED CROSS-SECTION OF THE I.F.T.

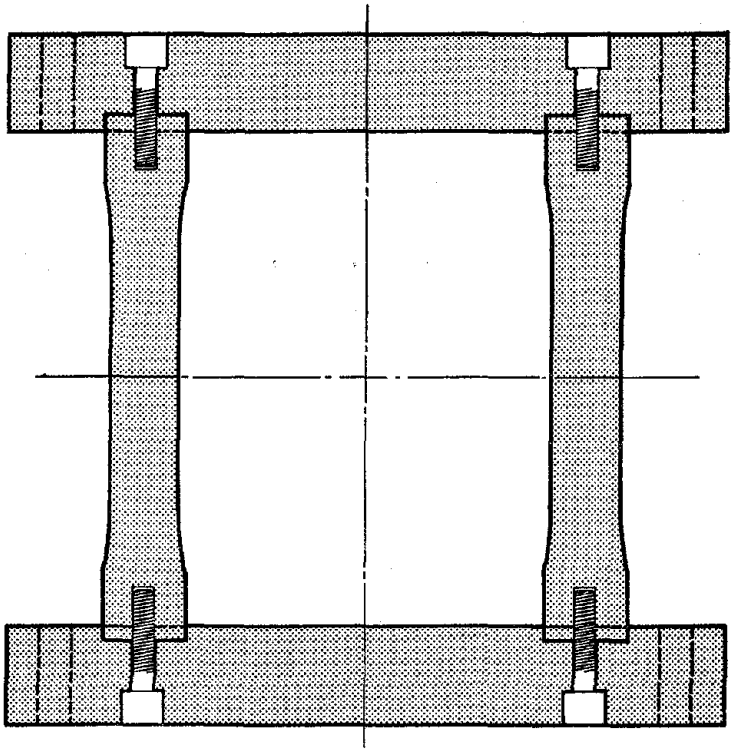

FIG. 2-6 VERTICAL SECTION OF THE ORIGINAL DESIGN SHOWING THE SCREWED CONNECTION BETWEEN THE I.F.T. AND END PLATES.

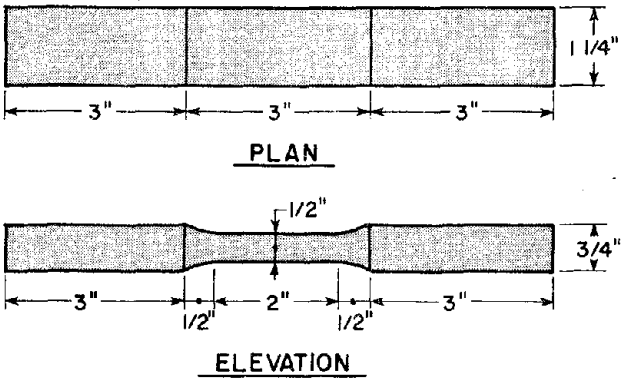

FIG. 2-7 SAMPLE OF I.F.T. PLATE MATERIAL USED TO TEST THE MECHANICAL CHARACTERISTICS OF THE 6061 ALUMINUM AFTER HEAT TREATMENT.

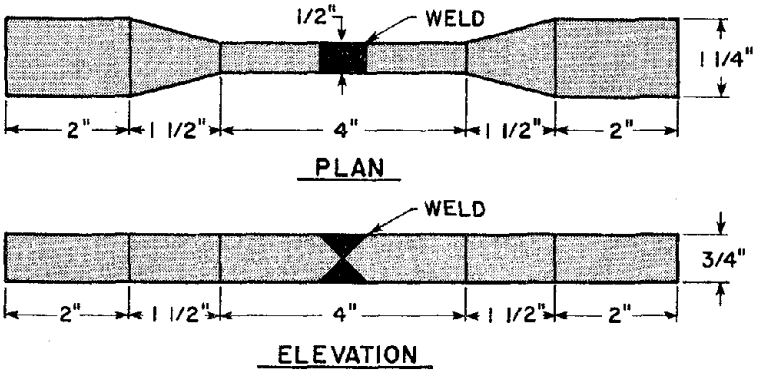

(a) SPECIMEN A

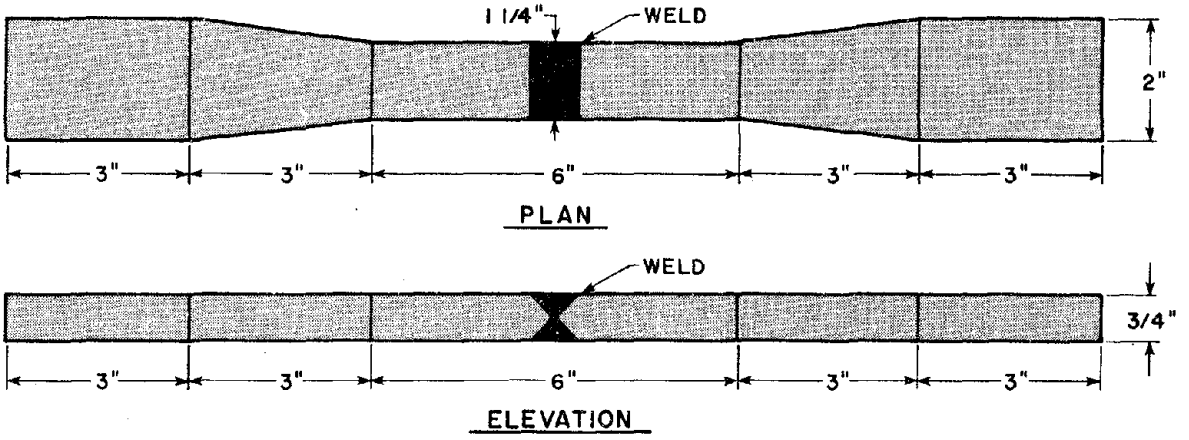

(b) SPECIMEN B

FIG. 2-8 SPECIMENS USED TO DETERMINE THE WELD STRENGTH.

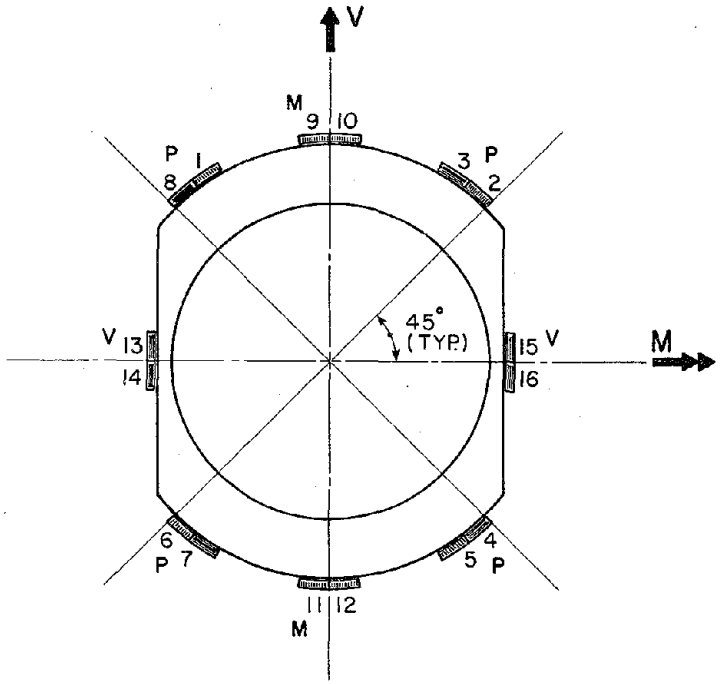

(a) GAGE LOCATIONS

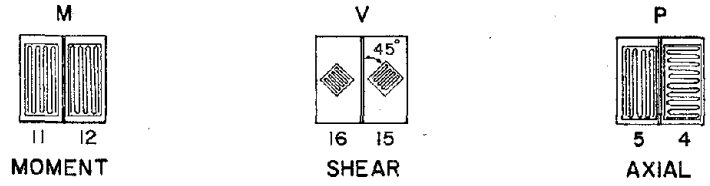

(b) GAGE ORIENTATIONS

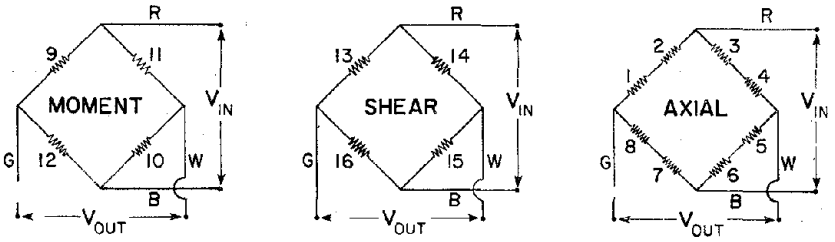

(c) WIRING SCHEMATIC

FIG. 2-9 INFORMATION ON GAGING OF INTERNAL FORCE TRANSDUCER.

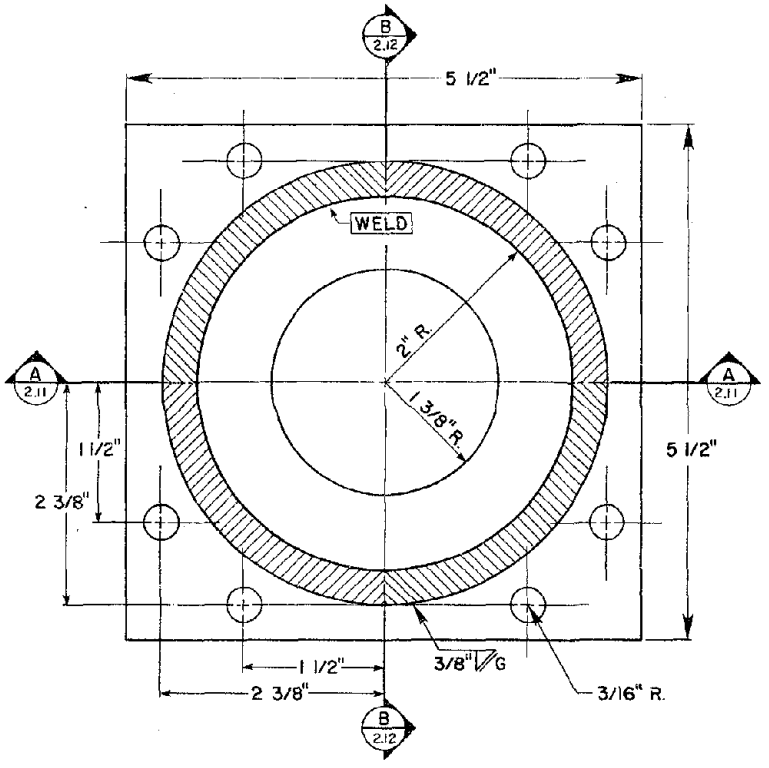

FIG. 2-10 PLAN OF THE I.F.T. END PLATE.

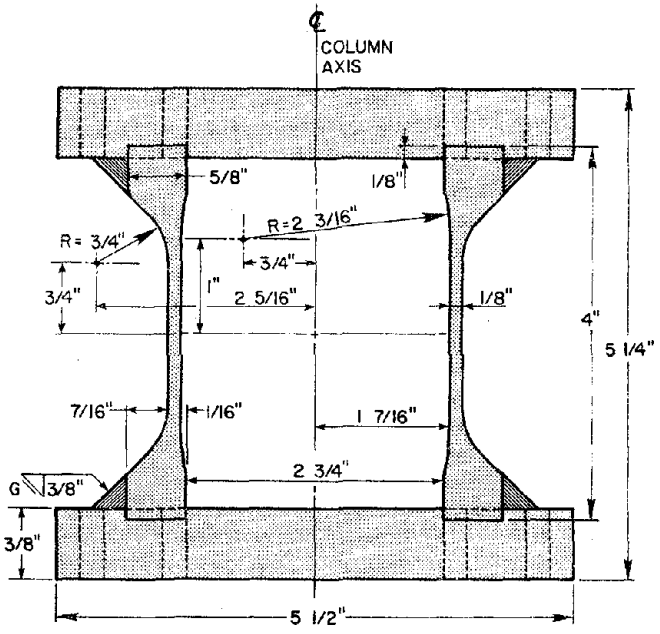

FIG. 2-11 SECTION A-A' OF THE I.F.T. (See Fig. 2-10) SHOWING THE SECTION MODIFICATION & WELDS.

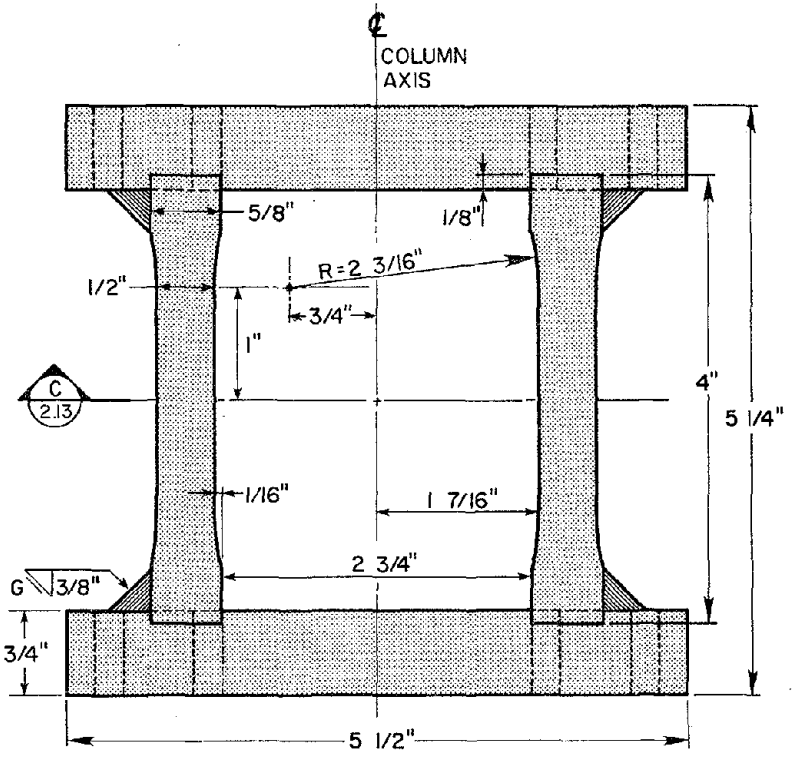

FIG. 2-12 SECTION B-B' OF THE I.F.T. (See Fig. 2-10)

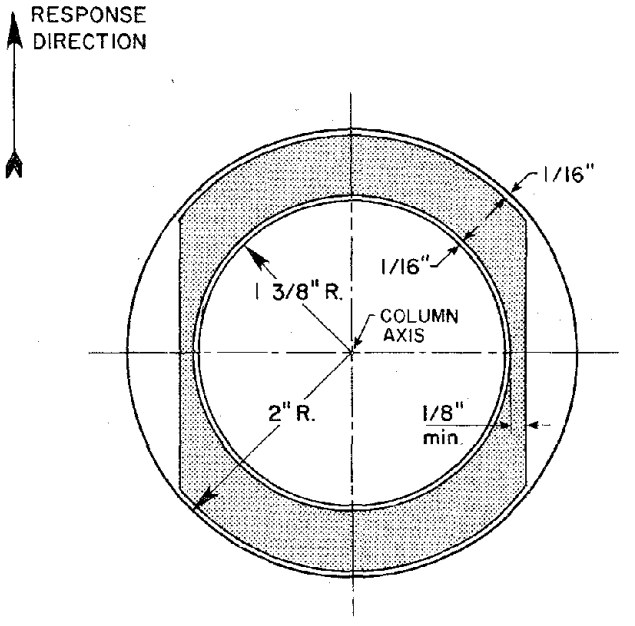

FIG. 2-13 SECTION C-C' OF THE I.F.T. (See Fig. 2-12)

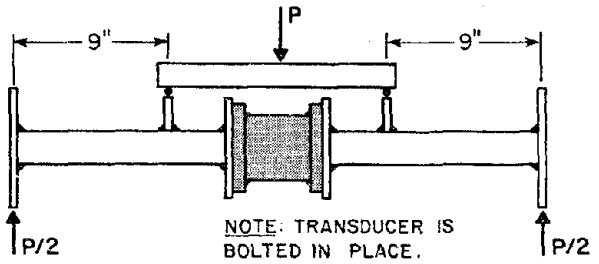

FIG. 3-1 ORIGINAL DEVICE USED FOR CALIBRATION OF THE I.F.T. MOMENT CHANNEL.

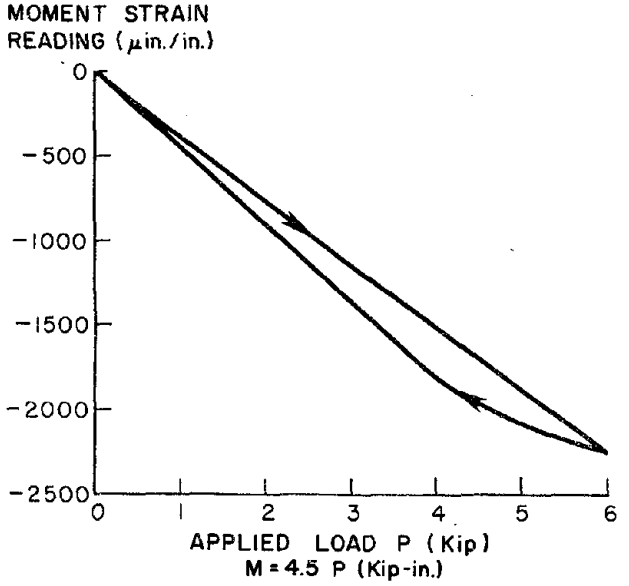

FIG. 3-2 TYPICAL CALIBRATION PLOT FOR AN I.F.T. MOMENT CHANNEL USING THE DEVICE IN FIG. 3-1.

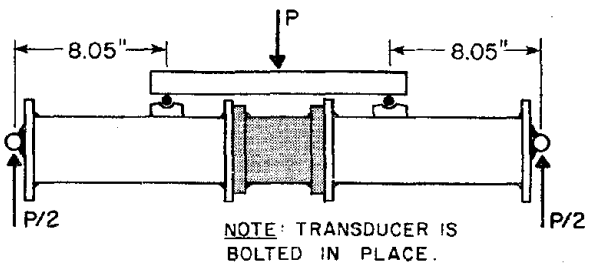

FIG. 3-3 IMPROVED DEVICE USED FOR CALIBRATION OF THE I.F.T. MOMENT CHANNEL.

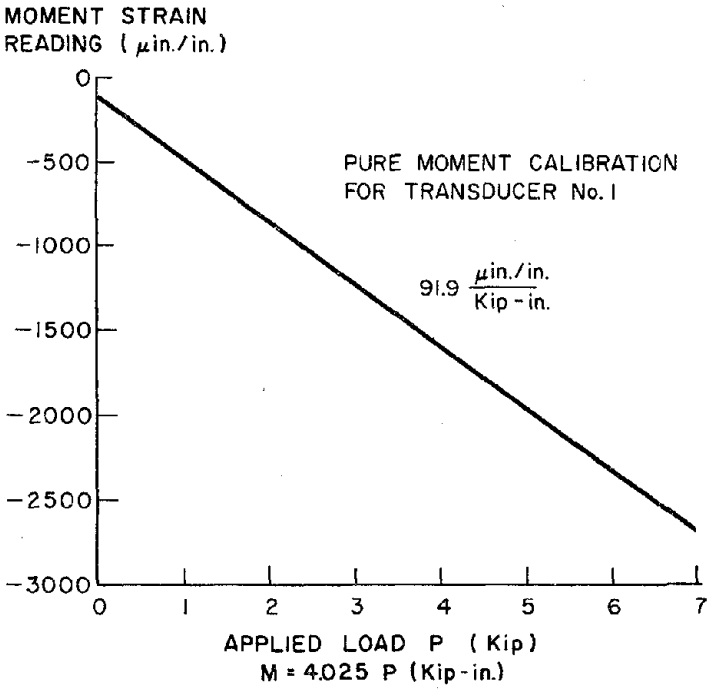

FIG. 3-4 TYPICAL CALIBRATION PLOT FOR AN I.F.T. MOMENT CHANNEL USING THE DEVICE SHOWN IN FIG. 3-3.

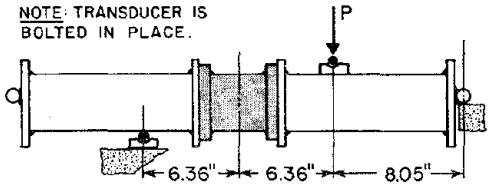

FIG. 3.5 DEVICE USED FOR COMBINED MOMENT-SHEAR CALIBRATION OF THE I.F.T.

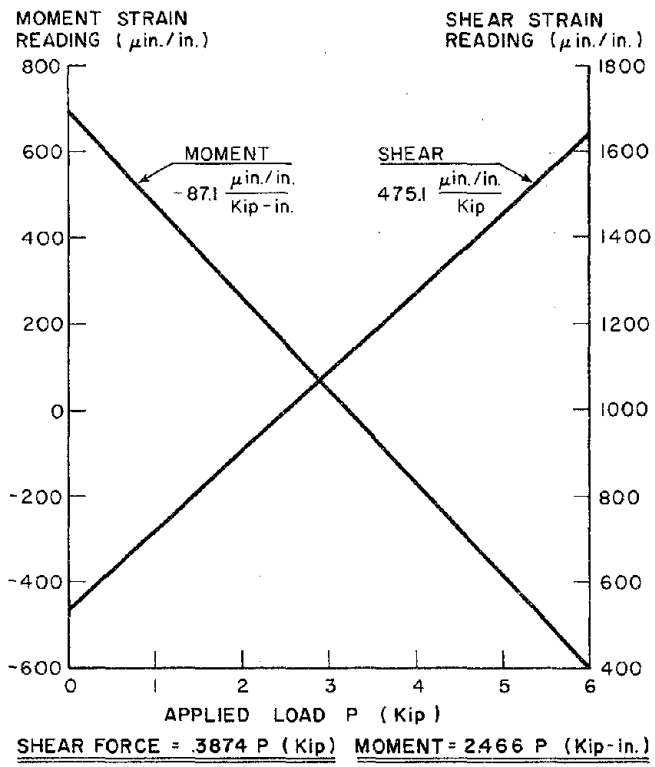

FIG. 3-6 TYPICAL CALIBRATION PLOT FOR COMBINED MOMENT-SHEAR LOADING OF AN I.F.T.

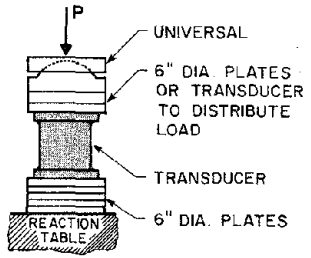

FIG. 3-7 SET-UP USED FOR AXIAL CALIBRATION OF A I.F.T.

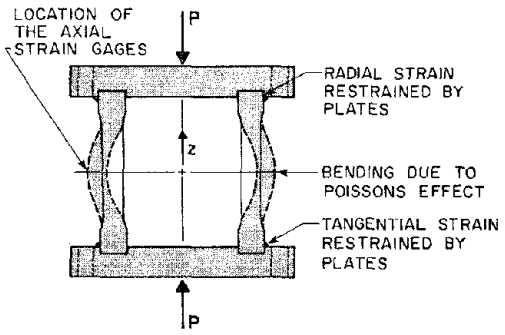

$\varepsilon_\theta = \frac{\nu}{E}\sigma_z$ IS RESTRAINED BY PLATES. STRAIN MEASURED BY LATERAL GAGES IS DECREASED.

$\varepsilon_r = \frac{\nu}{E}\sigma_z$ IS RESTRAINED BY PLATES AT THE ENDS OF THE TUBE, BUT NOT AT THE MIDDLE OF THE TUBE CAUSING BENDING.

ε_z AT THE LOCATION OF THE AXIAL STRAIN GAGES IS REDUCED BY THE BENDING.

FIG. 3-8 THE EFFECT OF END PLATE RESTRAINT ON THE I.F.T. STRAIN FIELD UNDER AXIAL LOADING.

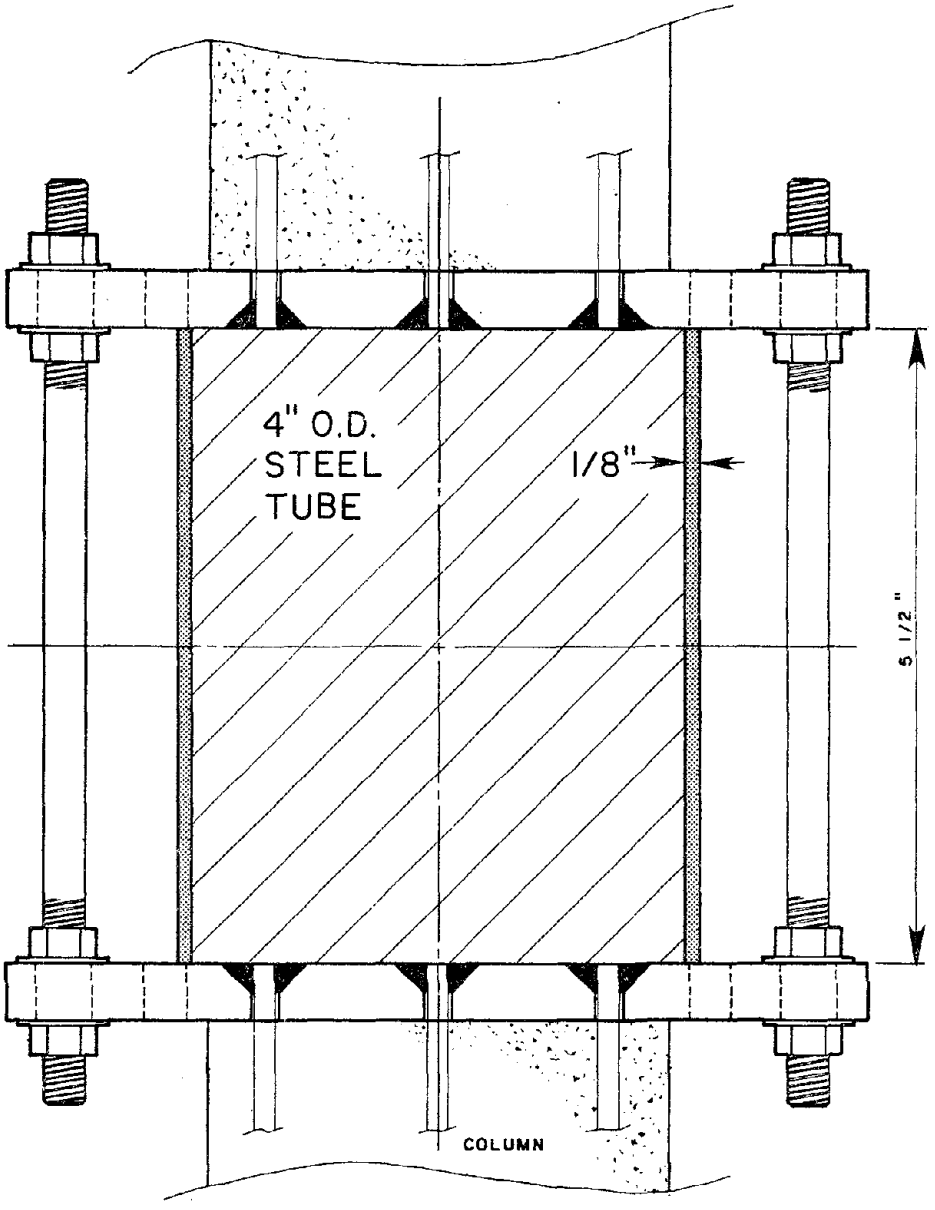

FIG. 4-1 LONGITUDINAL COLUMN SECTION SHOWING STEEL TUBE IN I.F.T. LOCATION DURING CONSTRUCTION.

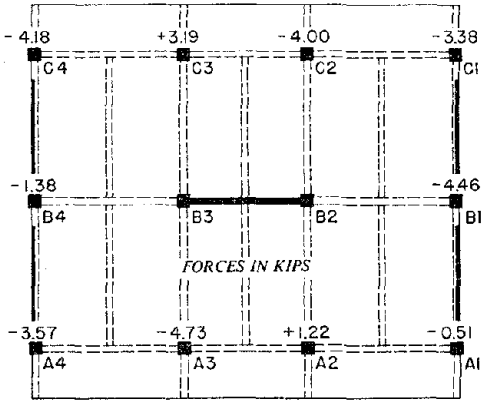

FIG. 4-2 MEASURED COLUMN LOADS AFTER INSTALLATION OF ALL I.F.T.s.

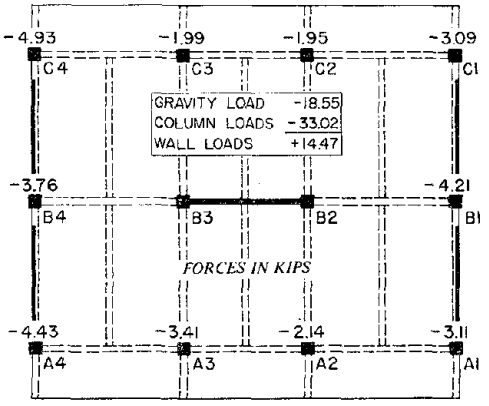

FIG. 4-3 MEASURED COLUMN LOAD AFTER EACH INDIVIDUAL I.F.T. WAS INSTALLED.

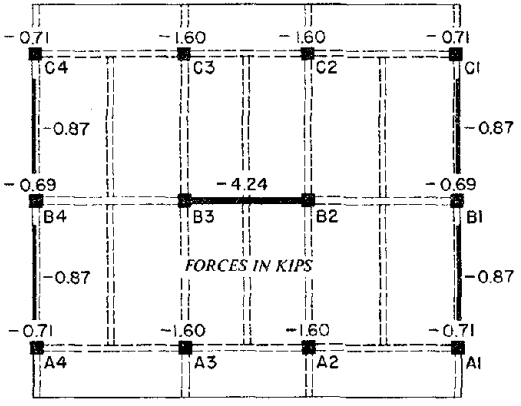

FIG. 4-4 CALCULATED GRAVITY LOADS FROM TRIBUTARY AREAS. [2]

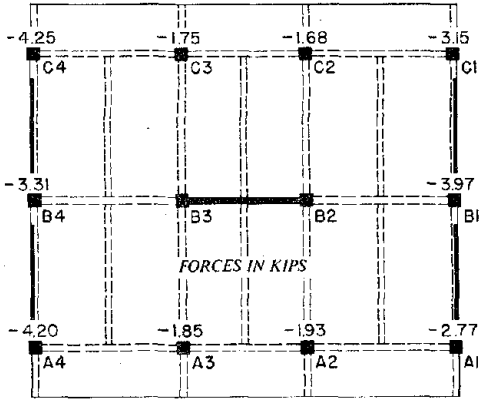

FIG. 4-5 ESTIMATED LOWER BOUND FOR COLUMN FORCES PRIOR TO I.F.T. INSTALLATION.

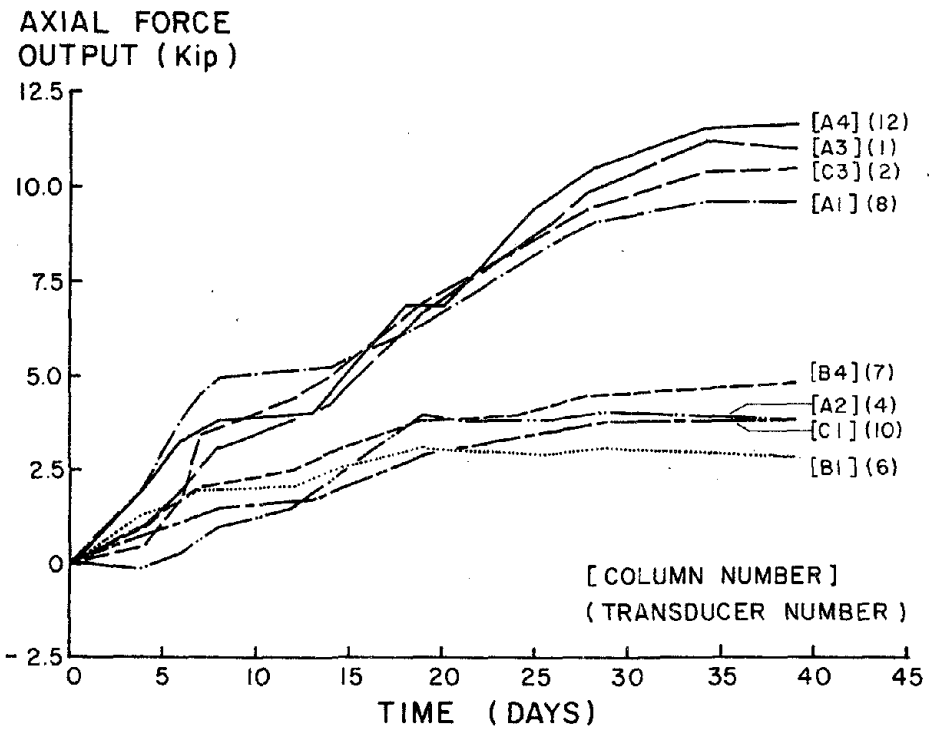

FIG. 4-6 DRIFT OF 8 I.F.T. AXIAL FORCE CHANNELS OVER 6 WEEKS.

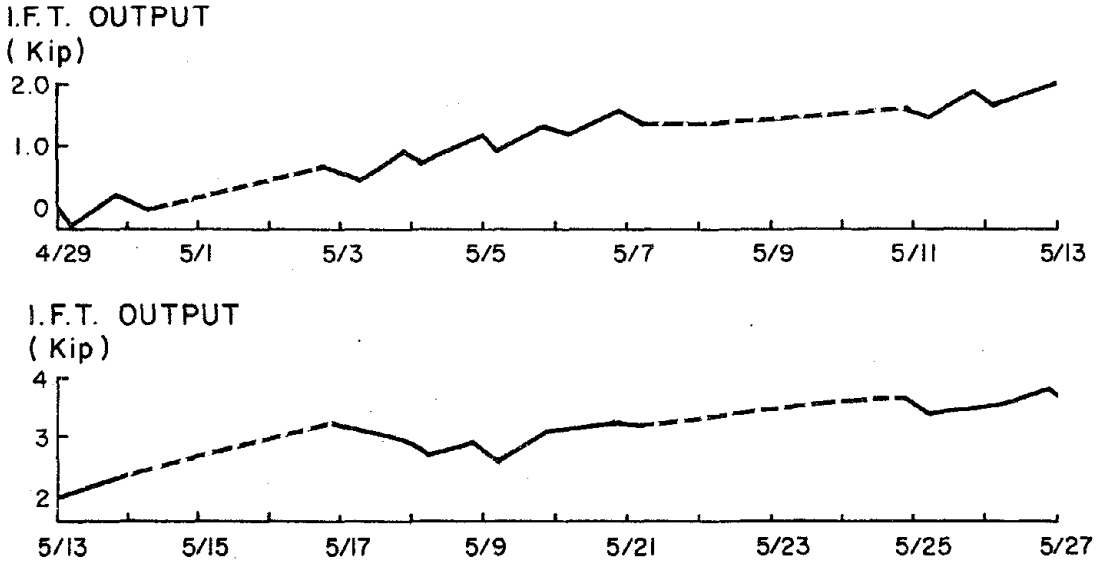

FIG. 4-7 DETAIL OF DRIFT OF THE AXIAL FORCE CHANNEL OF I.F.T. #10

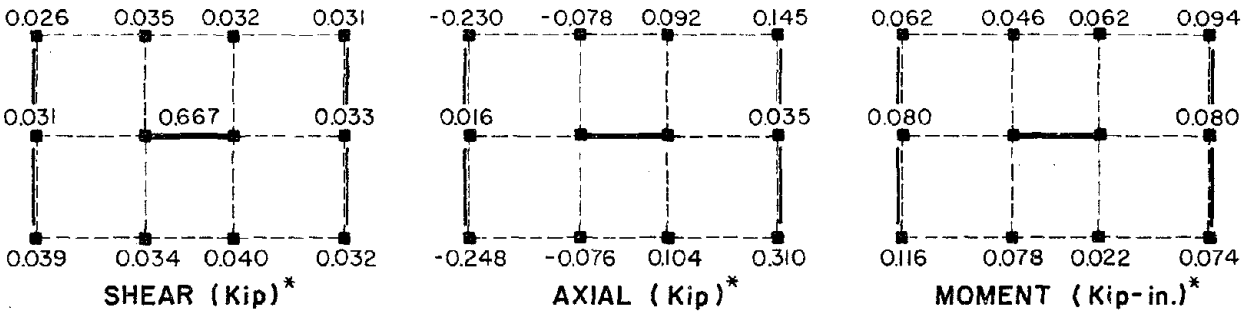

FIG. 4-8 EXAMPLE OF DATA ACQUIRED FROM I.F.T.s DURING THE FLEXIBILITY TESTS. THESE FORCE VALUES WERE OBTAINED DURING LOADING OF THE 7th FLOOR OF THE STRUCTURE WITHOUT BALLAST. [2]

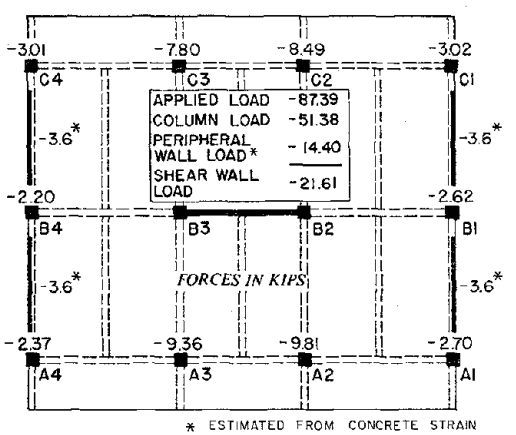

FIG. 4-9 DISTRIBUTION OF BALLAST LOAD FROM TRANSDUCER READINGS AND CONCRETE STRAIN GAGES.

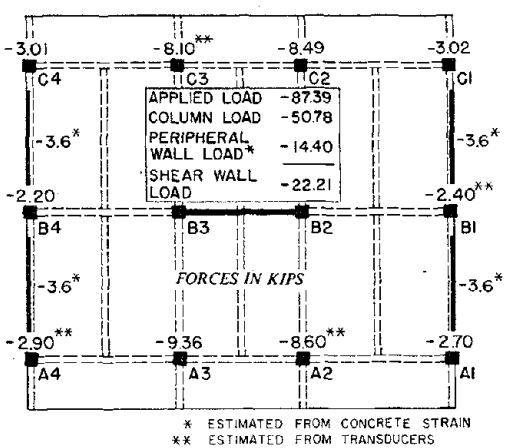

FIG. 4-10 ESTIMATED DISTRIBUTION OF BALLAST LOAD ACCOUNTING FOR TRANSDUCER DRIFT.

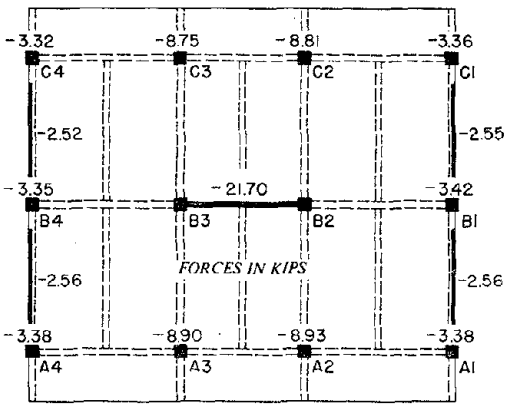

FIG. 4-11 CALCULATED DISTRIBUTION OF BALLAST LOAD FROM THE ACTUAL DISTRIBUTION OF BALLAST ON THE STRUCTURE. [8]

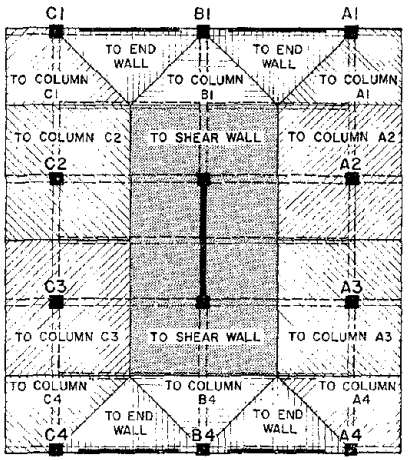

FIG. 4-12 TRIBUTARY AREAS USED BY CHOWDHURY. [Ref. 7]

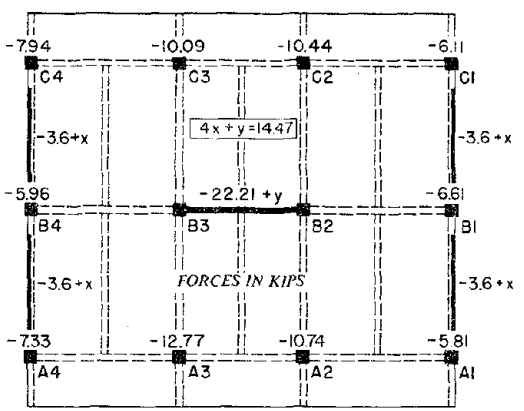

FIG. 4-13 DISTRIBUTION OF ALL STATIC LOAD FROM I.F.T.s. (See Fig. 4-3 & 4-10)

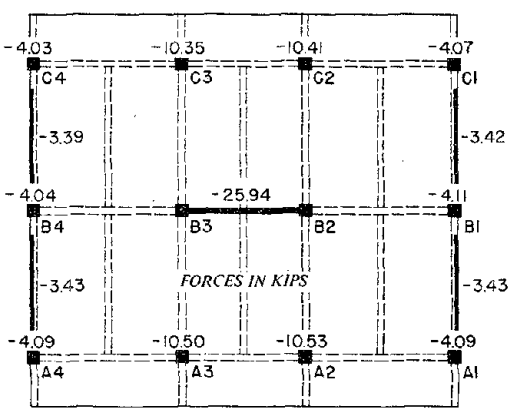

FIG. 4-14 CALCULATED DISTRIBUTION OF ALL STATIC LOAD. (See Fig. 4-4 & 4-11)

EARTHQUAKE ENGINEERING RESEARCH CENTER REPORTS

NOTE: Numbers in parentheses are Accession Numbers assigned by the National Technical Information Service; these are followed by a price code. Copies of the reports may be ordered from the National Technical Information Service, 5285 Port Royal Road, Springfield, Virginia, 22161. Accession Numbers should be quoted on orders for reports (PB --- ---) and remittance must accompany each order. Reports without this information were not available at time of printing. The complete list of EERC reports (from EERC 67-1) is available upon request from the Earthquake Engineering Research Center, University of California, Berkeley, 47th Street and Hoffman Boulevard, Richmond, California 94804.

UCB/EERC-77/01 "PLUSH - A Computer Program for Probabilistic Finite Element Analysis of Seismic Soil-Structure Interaction," by M.P. Romo Organista, J. Lysmer and H.B. Seed - 1977 (PB81 177 651)A05

UCB/EERC-77/02 "Soil-Structure Interaction Effects at the Humboldt Bay Power Plant in the Ferndale Earthquake of June 7, 1975," by J.E. Valera, H.B. Seed, C.F. Tsai and J. Lysmer - 1977 (PB 265 795)A04

UCB/EERC-77/03 "Influence of Sample Disturbance on Sand Response to Cyclic Loading," by K. Mori, H.B. Seed and C.K. Chan - 1977 (PB 267 352)A04

UCB/EERC-77/04 "Seismological Studies of Strong Motion Records," by J. Shoja-Taheri - 1977 (PB 269 655)A10

UCB/EERC-77/05 Unassigned

UCB/EERC-77/06 "Developing Methodologies for Evaluating the Earthquake Safety of Existing Buildings," by No. 1 - B. Bresler; No. 2 - B. Bresler, T. Okada and D. Zisling; No. 3 - T. Okada and B. Bresler; No. 4 - V.V. Bertero and B. Bresler - 1977 (PB 267 354)A08

UCB/EERC-77/07 "A Literature Survey - Transverse Strength of Masonry Walls," by Y. Omote, R.L. Mayes, S.W. Chen and R.W. Clough - 1977 (PB 277 933)A07

UCB/EERC-77/08 "DRAIN-TABS: A Computer Program for Inelastic Earthquake Response of Three Dimensional Buildings," by R. Guendelman-Israel and G.H. Powell - 1977 (PB 270 693)A07

UCB/EERC-77/09 "SUBWALL: A Special Purpose Finite Element Computer Program for Practical Elastic Analysis and Design of Structural Walls with Substructure Option," by D.Q. Le, H. Peterson and E.P. Popov - 1977 (PB 270 567)A05

UCB/EERC-77/10 "Experimental Evaluation of Seismic Design Methods for Broad Cylindrical Tanks," by D.P. Clough (PB 272 280)A13

UCB/EERC-77/11 "Earthquake Engineering Research at Berkeley - 1976," - 1977 (PB 273 507)A09

UCB/EERC-77/12 "Automated Design of Earthquake Resistant Multistory Steel Building Frames," by N.D. Walker, Jr. - 1977 (PB 276 526)A09

UCB/EERC-77/13 "Concrete Confined by Rectangular Hoops Subjected to Axial Loads," by J. Vallenas, V.V. Bertero and E.P. Popov - 1977 (PB 275 165)A06

UCB/EERC-77/14 "Seismic Strain Induced in the Ground During Earthquakes," by Y. Sugimura - 1977 (PB 284 201)A04

UCB/EERC-77/15 Unassigned

UCB/EERC-77/16 "Computer Aided Optimum Design of Ductile Reinforced Concrete Moment Resisting Frames," by S.W. Zagajeski and V.V. Bertero - 1977 (PB 280 137)A07

UCB/EERC-77/17 "Earthquake Simulation Testing of a Stepping Frame with Energy-Absorbing Devices," by J.M. Kelly and D.F. Tsztoo - 1977 (PB 273 506)A04

UCB/EERC-77/18 "Inelastic Behavior of Eccentrically Braced Steel Frames under Cyclic Loadings," by C.W. Roeder and E.P. Popov - 1977 (PB 275 526)A15

UCB/EERC-77/19 "A Simplified Procedure for Estimating Earthquake-Induced Deformations in Dams and Embankments," by F.I. Makdisi and H.B. Seed - 1977 (PB 276 820)A04

UCB/EERC-77/20 "The Performance of Earth Dams during Earthquakes," by H.B. Seed, F.I. Makdisi and P. de Alba - 1977 (PB 276 821)A04

UCB/EERC-77/21 "Dynamic Plastic Analysis Using Stress Resultant Finite Element Formulation," by P. Lukkunapvasit and J.M. Kelly - 1977 (PB 275 453)A04

UCB/EERC-77/22 "Preliminary Experimental Study of Seismic Uplift of a Steel Frame," by R.W. Clough and A.A. Huckelbridge 1977 (PB 278 769)A08

UCB/EERC-77/23 "Earthquake Simulator Tests of a Nine-Story Steel Frame with Columns Allowed to Uplift," by A.A. Huckelbridge - 1977 (PB 277 944)A09

UCB/EERC-77/24 "Nonlinear Soil-Structure Interaction of Skew Highway Bridges," by M.-C. Chen and J. Penzien - 1977 (PB 276 176)A07

UCB/EERC-77/25 "Seismic Analysis of an Offshore Structure Supported on Pile Foundations," by D.D.-N. Liou and J. Penzien 1977 (PB 283 180)A06

UCB/EERC-77/26 "Dynamic Stiffness Matrices for Homogeneous Viscoelastic Half-Planes," by G. Dasgupta and A.K. Chopra - 1977 (PB 279 654)A06

UCB/EERC-77/27 "A Practical Soft Story Earthquake Isolation System," by J.M. Kelly, J.M. Eidinger and C.J. Derham - 1977 (PB 276 814)A07

UCB/EERC-77/28 "Seismic Safety of Existing Buildings and Incentives for Hazard Mitigation in San Francisco: An Exploratory Study," by A.J. Meltsner - 1977 (PB 281 970)A05

UCB/EERC-77/29 "Dynamic Analysis of Electrohydraulic Shaking Tables," by D. Rea, S. Abedi-Hayati and Y. Takahashi 1977 (PB 282 569)A04

UCB/EERC-77/30 "An Approach for Improving Seismic - Resistant Behavior of Reinforced Concrete Interior Joints," by B. Galunic, V.V. Bertero and E.P. Popov - 1977 (PB 290 870)A06

UCB/EERC-78/01 "The Development of Energy-Absorbing Devices for Aseismic Base Isolation Systems," by J.M. Kelly and D.F. Tsztoo - 1978 (PB 284 978)A04

UCB/EERC-78/02 "Effect of Tensile Prestrain on the Cyclic Response of Structural Steel Connections, by J.G. Bouwkamp and A. Mukhopadhyay - 1978

UCB/EERC-78/03 "Experimental Results of an Earthquake Isolation System using Natural Rubber Bearings," by J.M. Eidinger and J.M. Kelly - 1978 (PB 281 686)A04

UCB/EERC-78/04 "Seismic Behavior of Tall Liquid Storage Tanks," by A. Niwa - 1978 (PB 284 017)A14

UCB/EERC-78/05 "Hysteretic Behavior of Reinforced Concrete Columns Subjected to High Axial and Cyclic Shear Forces," by S.W. Zagajeski, V.V. Bertero and J.G. Bouwkamp - 1978 (PB 283 858)A13

UCB/EERC-78/06 "Three Dimensional Inelastic Frame Elements for the ANSR-I Program," by A. Riahi, D.G. Row and G.H. Powell - 1978 (PB 295 755)A04

UCB/EERC-78/07 "Studies of Structural Response to Earthquake Ground Motion," by O.A. Lopez and A.K. Chopra - 1978 (PB 282 790)A05

UCB/EERC-78/08 "A Laboratory Study of the Fluid-Structure Interaction of Submerged Tanks and Caissons in Earthquakes," by R.C. Byrd - 1978 (PB 284 957)A08

UCB/EERC-78/09 Unassigned

UCB/EERC-78/10 "Seismic Performance of Nonstructural and Secondary Structural Elements," by I. Sakamoto - 1978 (PB81 154 593)A05

UCB/EERC-78/11 "Mathematical Modelling of Hysteresis Loops for Reinforced Concrete Columns," by S. Nakata, T. Sproul and J. Penzien - 1978 (PB 298 274)A05

UCB/EERC-78/12 "Damageability in Existing Buildings," by T. Blejwas and B. Bresler - 1978 (PB 80 166 978)A05

UCB/EERC-78/13 "Dynamic Behavior of a Pedestal Base Multistory Building," by R.M. Stephen, E.L. Wilson, J.G. Bouwkamp and M. Button - 1978 (PB 286 650)A08

UCB/EERC-78/14 "Seismic Response of Bridges - Case Studies," by R.A. Imbsen, V. Nutt and J. Penzien - 1978 (PB 286 503)A10

UCB/EERC-78/15 "A Substructure Technique for Nonlinear Static and Dynamic Analysis," by D.G. Row and G.H. Powell - 1978 (PB 288 077)A10

UCB/EERC-78/16 "Seismic Risk Studies for San Francisco and for the Greater San Francisco Bay Area," by C.S. Oliveira - 1978 (PB 81 120 115)A07

UCB/EERC-78/17 "Strength of Timber Roof Connections Subjected to Cyclic Loads," by P. Gülkan, R.L. Mayes and R.W. Clough - 1978 (HUD-000 1491)A07

UCB/EERC-78/18 "Response of K-Braced Steel Frame Models to Lateral Loads," by J.G. Bouwkamp, R.M. Stephen and E.P. Popov - 1978

UCB/EERC-78/19 "Rational Design Methods for Light Equipment in Structures Subjected to Ground Motion," by J.L. Sackman and J.M. Kelly - 1978 (PB 292 357)A04

UCB/EERC-78/20 "Testing of a Wind Restraint for Aseismic Base Isolation," by J.M. Kelly and D.E. Chitty - 1978 (PB 292 833)A03

UCB/EERC-78/21 "APOLLO - A Computer Program for the Analysis of Pore Pressure Generation and Dissipation in Horizontal Sand Layers During Cyclic or Earthquake Loading," by P.P. Martin and H.B. Seed - 1978 (PB 292 835)A04

UCB/EERC-78/22 "Optimal Design of an Earthquake Isolation System," by M.A. Bhatti, K.S. Pister and E. Polak - 1978 (PB 294 735)A06

UCB/EERC-78/23 "MASH - A Computer Program for the Non-Linear Analysis of Vertically Propagating Shear Waves in Horizontally Layered Deposits," by P.P. Martin and H.B. Seed - 1978 (PB 293 101)A05

UCB/EERC-78/24 "Investigation of the Elastic Characteristics of a Three Story Steel Frame Using System Identification," by I. Kaya and H.D. McNiven - 1978 (PB 296 225)A06

UCB/EERC-78/25 "Investigation of the Nonlinear Characteristics of a Three-Story Steel Frame Using System Identification," by I. Kaya and H.D. McNiven - 1978 (PB 301 363)A05

UCB/EERC-78/26 "Studies of Strong Ground Motion in Taiwan," by Y.M. Hsiung, B.A. Bolt and J. Penzien - 1978 (PB 298 436)A06

UCB/EERC-78/27 "Cyclic Loading Tests of Masonry Single Piers: Volume 1 - Height to Width Ratio of 2," by P.A. Hidalgo, R.L. Mayes, H.D. McNiven and R.W. Clough - 1978 (PB 296 211)A07

UCB/EERC-78/28 "Cyclic Loading Tests of Masonry Single Piers: Volume 2 - Height to Width Ratio of 1," by S.-W.J. Chen, P.A. Hidalgo, R.L. Mayes, R.W. Clough and H.D. McNiven - 1978 (PB 296 212)A09

UCB/EERC-78/29 "Analytical Procedures in Soil Dynamics," by J. Lysmer - 1978 (PB 298 445)A06

UCB/EERC-79/01 "Hysteretic Behavior of Lightweight Reinforced Concrete Beam-Column Subassemblages," by B. Forzani, E.P. Popov and V.V. Bertero - April 1979(PB 298 267)A06

UCB/EERC-79/02 "The Development of a Mathematical Model to Predict the Flexural Response of Reinforced Concrete Beams to Cyclic Loads, Using System Identification," by J. Stanton & H. McNiven - Jan. 1979(PB 295 875)A10

UCB/EERC-79/03 "Linear and Nonlinear Earthquake Response of Simple Torsionally Coupled Systems," by C.L. Kan and A.K. Chopra - Feb. 1979(PB 298 262)A06

UCB/EERC-79/04 "A Mathematical Model of Masonry for Predicting its Linear Seismic Response Characteristics," by Y. Mengi and H.D. McNiven - Feb. 1979(PB 298 266)A06

UCB/EERC-79/05 "Mechanical Behavior of Lightweight Concrete Confined by Different Types of Lateral Reinforcement," by M.A. Manrique, V.V. Bertero and E.P. Popov - May 1979(PB 301 114)A06

UCB/EERC-79/06 "Static Tilt Tests of a Tall Cylindrical Liquid Storage Tank," by R.W. Clough and A. Niwa - Feb. 1979 (PB 301 167)A06

UCB/EERC-79/07 "The Design of Steel Energy Absorbing Restrainers and Their Incorporation into Nuclear Power Plants for Enhanced Safety: Volume 1 - Summary Report," by P.N. Spencer, V.F. Zackay, and E.R. Parker - Feb. 1979(UCB/EERC-79/07)A09

UCB/EERC-79/08 "The Design of Steel Energy Absorbing Restrainers and Their Incorporation into Nuclear Power Plants for Enhanced Safety: Volume 2 - The Development of Analyses for Reactor System Piping,""Simple Systems" by M.C. Lee, J. Penzien, A.K. Chopra and K, Suzuki "Complex Systems" by G.H. Powell, E.L. Wilson, R.W. Clough and D.G. Row - Feb. 1979(UCB/EERC-79/08)A10

UCB/EERC-79/09 "The Design of Steel Energy Absorbing Restrainers and Their Incorporation into Nuclear Power Plants for Enhanced Safety: Volume 3 - Evaluation of Commercial Steels," by W.S. Owen, R.M.N. Pelloux, R.O. Ritchie, M. Faral, T. Ohhashi, J. Toplosky, S.J. Hartman, V.F. Zackay and E.R. Parker - Feb. 1979(UCB/EERC-79/09)A04

UCB/EERC-79/10 "The Design of Steel Energy Absorbing Restrainers and Their Incorporation into Nuclear Power Plants for Enhanced Safety: Volume 4 - A Review of Energy-Absorbing Devices," by J.M. Kelly and M.S. Skinner - Feb. 1979(UCB/EERC-79/10)A04

UCB/EERC-79/11 "Conservatism In Summation Rules for Closely Spaced Modes," by J.M. Kelly and J.L. Sackman - May 1979(PB 301 328)A03

UCB/EERC-79/12 "Cyclic Loading Tests of Masonry Single Piers; Volume 3 - Height to Width Ratio of 0.5," by P.A. Hidalgo, R.L. Mayes, H.D. McNiven and R.W. Clough - May 1979(PB 301 321)A08

UCB/EERC-79/13 "Cyclic Behavior of Dense Course-Grained Materials in Relation to the Seismic Stability of Dams," by N.G. Banerjee, H.B. Seed and C.K. Chan - June 1979(PB 301 373)A13

UCB/EERC-79/14 "Seismic Behavior of Reinforced Concrete Interior Beam-Column Subassemblages," by S. Viwathanatepa, E.P. Popov and V.V. Bertero - June 1979(PB 301 326)A10

UCB/EERC-79/15 "Optimal Design of Localized Nonlinear Systems with Dual Performance Criteria Under Earthquake Excitations," by M.A. Bhatti - July 1979(PB 80 167 109)A06

UCB/EERC-79/16 "OPTDYN - A General Purpose Optimization Program for Problems with or without Dynamic Constraints," by M.A. Bhatti, E. Polak and K.S. Pister - July 1979(PB 80 167 091)A05

UCB/EERC-79/17 "ANSR-II, Analysis of Nonlinear Structural Response, Users Manual," by D.P. Mondkar and G.H. Powell July 1979(PB 80 113 301)A05

UCB/EERC-79/18 "Soil Structure Interaction in Different Seismic Environments," A. Gomez-Masso, J. Lysmer, J.-C. Chen and H.B. Seed - August 1979(PB 80 101 520)A04

UCB/EERC-79/19 "ARMA Models for Earthquake Ground Motions," by M.K. Chang, J.W. Kwiatkowski, R.F. Nau, R.M. Oliver and K.S. Pister - July 1979(PB 301 166)A05

UCB/EERC-79/20 "Hysteretic Behavior of Reinforced Concrete Structural Walls," by J.M. Vallenas, V.V. Bertero and E.P. Popov - August 1979(PB 80 165 905)A12

UCB/EERC-79/21 "Studies on High-Frequency Vibrations of Buildings - 1: The Column Effect," by J. Lubliner - August 1979 (PB 80 158 553)A03

UCB/EERC-79/22 "Effects of Generalized Loadings on Bond Reinforcing Bars Embedded in Confined Concrete Blocks," by S. Viwathanatepa, E.P. Popov and V.V. Bertero - August 1979(PB 81 124 018)A14

UCB/EERC-79/23 "Shaking Table Study of Single-Story Masonry Houses, Volume 1: Test Structures 1 and 2," by P. Gülkan, R.L. Mayes and R.W. Clough - Sept. 1979 (HUD-000 1763)A12

UCB/EERC-79/24 "Shaking Table Study of Single-Story Masonry Houses, Volume 2: Test Structures 3 and 4," by P. Gülkan, R.L. Mayes and R.W. Clough - Sept. 1979 (HUD-000 1836)A12

UCB/EERC-79/25 "Shaking Table Study of Single-Story Masonry Houses, Volume 3: Summary, Conclusions and Recommendations," by R.W. Clough, R.L. Mayes and P. Gülkan - Sept. 1979 (HUD-000 1837)A06

UCB/EERC-79/26 "Recommendations for a U.S.-Japan Cooperative Research Program Utilizing Large-Scale Testing Facilities," by U.S.-Japan Planning Group - Sept. 1979(PB 301 407)A06

UCB/EERC-79/27 "Earthquake-Induced Liquefaction Near Lake Amatitlan, Guatemala," by H.B. Seed, I. Arango, C.K. Chan, A. Gomez-Masso and R. Grant de Ascoli - Sept. 1979(NUREG-CR1341)A03

UCB/EERC-79/28 "Infill Panels: Their Influence on Seismic Response of Buildings," by J.W. Axley and V.V. Bertero Sept. 1979(PB 80 163 371)A10

UCB/EERC-79/29 "3D Truss Bar Element (Type 1) for the ANSR-II Program," by D.P. Mondkar and G.H. Powell - Nov. 1979 (PB 80 169 709)A02

UCB/EERC-79/30 "2D Beam-Column Element (Type 5 - Parallel Element Theory) for the ANSR-II Program," by D.G. Row, G.H. Powell and D.P. Mondkar - Dec. 1979(PB 80 167 224)A03

UCB/EERC-79/31 "3D Beam-Column Element (Type 2 - Parallel Element Theory) for the ANSR-II Program," by A. Riahi, G.H. Powell and D.P. Mondkar - Dec. 1979(PB 80 167 216)A03

UCB/EERC-79/32 "On Response of Structures to Stationary Excitation," by A. Der Kiureghian - Dec. 1979(PB 80166 929)A03

UCB/EERC-79/33 "Undisturbed Sampling and Cyclic Load Testing of Sands," by S. Singh, H.B. Seed and C.K. Chan Dec. 1979(ADA 087 298)A07

UCB/EERC-79/34 "Interaction Effects of Simultaneous Torsional and Compressional Cyclic Loading of Sand," by P.M. Griffin and W.N. Houston - Dec. 1979(ADA 092 352)A15

UCB/EERC-80/01 "Earthquake Response of Concrete Gravity Dams Including Hydrodynamic and Foundation Interaction Effects," by A.K. Chopra, P. Chakrabarti and S. Gupta - Jan. 1980(AD-A087297)A10

UCB/EERC-80/02 "Rocking Response of Rigid Blocks to Earthquakes," by C.S. Yim, A.K. Chopra and J. Penzien - Jan. 1980 (PB80 166 002)A04

UCB/EERC-80/03 "Optimum Inelastic Design of Seismic-Resistant Reinforced Concrete Frame Structures," by S.W. Zagajeski and V.V. Bertero - Jan. 1980(PB80 164 635)A06

UCB/EERC-80/04 "Effects of Amount and Arrangement of Wall-Panel Reinforcement on Hysteretic Behavior of Reinforced Concrete Walls," by R. Iliya and V.V. Bertero - Feb. 1980(PB81 122 525)A09

UCB/EERC-80/05 "Shaking Table Research on Concrete Dam Models," by A. Niwa and R.W. Clough - Sept. 1980(PB81 122 368)A06

UCB/EERC-80/06 "The Design of Steel Energy-Absorbing Restrainers and their Incorporation into Nuclear Power Plants for Enhanced Safety (Vol 1A): Piping with Energy Absorbing Restrainers: Parameter Study on Small Systems," by G.H. Powell, C. Oughourlian and J. Simons - June 1980

UCB/EERC-80/07 "Inelastic Torsional Response of Structures Subjected to Earthquake Ground Motions," by Y. Yamazaki April 1980(PB81 122 327)A08

UCB/EERC-80/08 "Study of X-Braced Steel Frame Structures Under Earthquake Simulation," by Y. Ghanaat - April 1980 (PB81 122 335)A11

UCB/EERC-80/09 "Hybrid Modelling of Soil-Structure Interaction," by S. Gupta, T.W. Lin, J. Penzien and C.S. Yeh May 1980(PB81 122 319)A07

UCB/EERC-80/10 "General Applicability of a Nonlinear Model of a One Story Steel Frame," by B.I. Sveinsson and H.D. McNiven - May 1980(PB81 124 877)A06

UCB/EERC-80/11 "A Green-Function Method for Wave Interaction with a Submerged Body," by W. Kioka - April 1980 (PB81 122 269)A07

UCB/EERC-80/12 "Hydrodynamic Pressure and Added Mass for Axisymmetric Bodies," by F. Nilrat - May 1980(PB81 122 343)A08

UCB/EERC-80/13 "Treatment of Non-Linear Drag Forces Acting on Offshore Platforms," by B.V. Dao and J. Penzien May 1980(PB81 153 413)A07

UCB/EERC-80/14 "2D Plane/Axisymmetric Solid Element (Type 3 - Elastic or Elastic-Perfectly Plastic) for the ANSR-II Program," by D.P. Mondkar and G.H. Powell - July 1980(PB81 122 350)A03

UCB/EERC-80/15 "A Response Spectrum Method for Random Vibrations," by A. Der Kiureghian - June 1980(PB81 122 301)A03

UCB/EERC-80/16 "Cyclic Inelastic Buckling of Tubular Steel Braces," by V.A. Zayas, E.P. Popov and S.A. Mahin June 1980(PB81 124 885)A10

UCB/EERC-80/17 "Dynamic Response of Simple Arch Dams Including Hydrodynamic Interaction," by C.S. Porter and A.K. Chopra - July 1980(PB81 124 000)A13

UCB/EERC-80/18 "Experimental Testing of a Friction Damped Aseismic Base Isolation System with Fail-Safe Characteristics," by J.M. Kelly, K.E. Beucke and M.S. Skinner - July 1980(PB81 148 595)A04

UCB/EERC-80/19 "The Design of Steel Energy-Absorbing Restrainers and their Incorporation into Nuclear Power Plants for Enhanced Safety (Vol 1B): Stochastic Seismic Analyses of Nuclear Power Plant Structures and Piping Systems Subjected to Multiple Support Excitations," by M.C. Lee and J. Penzien - June 1980

UCB/EERC-80/20 "The Design of Steel Energy-Absorbing Restrainers and their Incorporation into Nuclear Power Plants for Enhanced Safety (Vol 1C): Numerical Method for Dynamic Substructure Analysis," by J.M. Dickens and E.L. Wilson - June 1980

UCB/EERC-80/21 "The Design of Steel Energy-Absorbing Restrainers and their Incorporation into Nuclear Power Plants for Enhanced Safety (Vol 2): Development and Testing of Restraints for Nuclear Piping Systems," by J.M. Kelly and M.S. Skinner - June 1980

UCB/EERC-80/22 "3D Solid Element (Type 4-Elastic or Elastic-Perfectly-Plastic) for the ANSR-II Program," by D.P. Mondkar and G.H. Powell - July 1980(PB81 123 242)A03

UCB/EERC-80/23 "Gap-Friction Element (Type 5) for the ANSR-II Program," by D.P. Mondkar and G.H. Powell - July 1980 (PB81 122 285)A03

UCB/EERC-80/24 "U-Bar Restraint Element (Type 11) for the ANSR-II Program," by C. Oughourlian and G.H. Powell July 1980(PB81 122 293)A03

UCB/EERC-80/25 "Testing of a Natural Rubber Base Isolation System by an Explosively Simulated Earthquake," by J.M. Kelly - August 1980(PB81 201 360)A04

UCB/EERC-80/26 "Input Identification from Structural Vibrational Response," by Y. Hu - August 1980(PB81 152 308)A05

UCB/EERC-80/27 "Cyclic Inelastic Behavior of Steel Offshore Structures," by V.A. Zayas, S.A. Mahin and E.P. Popov August 1980(PB81 196 180)A15

UCB/EERC-80/28 "Shaking Table Testing of a Reinforced Concrete Frame with Biaxial Response," by M.G. Oliva October 1980(PB81 154 304)A10

UCB/EERC-80/29 "Dynamic Properties of a Twelve-Story Prefabricated Panel Building," by J.G. Bouwkamp, J.P. Kollegger and R.M. Stephen - October 1980(PB82 117 128)A06

UCB/EERC-80/30 "Dynamic Properties of an Eight-Story Prefabricated Panel Building," by J.G. Bouwkamp, J.P. Kollegger and R.M. Stephen - October 1980(PB81 200 313)A05

UCB/EERC-80/31 "Predictive Dynamic Response of Panel Type Structures Under Earthquakes," by J.P. Kollegger and J.G. Bouwkamp - October 1980(PB81 152 316)A04

UCB/EERC-80/32 "The Design of Steel Energy-Absorbing Restrainers and their Incorporation into Nuclear Power Plants for Enhanced Safety (Vol 3): Testing of Commercial Steels in Low-Cycle Torsional Fatigue," by P. Spencer, E.R. Parker, E. Jongewaard and M. Drory

UCB/EERC-80/33 "The Design of Steel Energy-Absorbing Restrainers and their Incorporation into Nuclear Power Plants for Enhanced Safety (Vol 4): Shaking Table Tests of Piping Systems with Energy-Absorbing Restrainers," by S.F. Stiemer and W.G. Godden - Sept. 1980

UCB/EERC-80/34 "The Design of Steel Energy-Absorbing Restrainers and their Incorporation into Nuclear Power Plants for Enhanced Safety (Vol 5): Summary Report," by P. Spencer

UCB/EERC-80/35 "Experimental Testing of an Energy-Absorbing Base Isolation System," by J.M. Kelly, M.S. Skinner and K.E. Beucke - October 1980(PB81 154 072)A04

UCB/EERC-80/36 "Simulating and Analyzing Artificial Non-Stationary Earthquake Ground Motions," by R.F. Nau, R.M. Oliver and K.S. Pister - October 1980(PB81 153 397)A04

UCB/EERC-80/37 "Earthquake Engineering at Berkeley - 1980," - Sept. 1980(PB81 205 874)A09

UCB/EERC-80/38 "Inelastic Seismic Analysis of Large Panel Buildings," by V. Schricker and G.H. Powell - Sept. 1980 (PB81 154 338)A13

UCB/EERC-80/39 "Dynamic Response of Embankment, Concrete-Gravity and Arch Dams Including Hydrodynamic Interaction," by J.F. Hall and A.K. Chopra - October 1980(PB81 152 324)A11

UCB/EERC-80/40 "Inelastic Buckling of Steel Struts Under Cyclic Load Reversal," by R.G. Black, W.A. Wenger and E.P. Popov - October 1980(PB81 154 312)A08

UCB/EERC-80/41 "Influence of Site Characteristics on Building Damage During the October 3, 1974 Lima Earthquake," by P. Repetto, I. Arango and H.B. Seed - Sept. 1980(PB81 161 739)A05

UCB/EERC-80/42 "Evaluation of a Shaking Table Test Program on Response Behavior of a Two Story Reinforced Concrete Frame," by J.M. Blondet, R.W. Clough and S.A. Mahin

UCB/EERC-80/43 "Modelling of Soil-Structure Interaction by Finite and Infinite Elements," by F. Medina - December 1980(PB81 229 270)A04

UCB/EERC-81/01 "Control of Seismic Response of Piping Systems and Other Structures by Base Isolation," edited by J.M. Kelly - January 1981 (PB81 200 735)A05

UCB/EERC-81/02 "OPTNSR - An Interactive Software System for Optimal Design of Statically and Dynamically Loaded Structures with Nonlinear Response," by M.A. Bhatti, V. Ciampi and K.S. Pister - January 1981 (PB81 218 851)A09

UCB/EERC-81/03 "Analysis of Local Variations in Free Field Seismic Ground Motions," by J.-C. Chen, J. Lysmer and H.B. Seed - January 1981 (AD-A099508)A13

UCB/EERC-81/04 "Inelastic Structural Modeling of Braced Offshore Platforms for Seismic Loading," by V.A. Zayas, P.-S.B. Shing, S.A. Mahin and E.P. Popov - January 1981(PB82 138 777)A07

UCB/EERC-81/05 "Dynamic Response of Light Equipment in Structures," by A. Der Kiureghian, J.L. Sackman and B. Nour-Omid - April 1981 (PB81 218 497)A04

UCB/EERC-81/06 "Preliminary Experimental Investigation of a Broad Base Liquid Storage Tank," by J.G. Bouwkamp, J.P. Kollegger and R.M. Stephen - May 1981(PB82 140 385)A03

UCB/EERC-81/07 "The Seismic Resistant Design of Reinforced Concrete Coupled Structural Walls," by A.E. Aktan and V.V. Bertero - June 1981(PB82 113 358)A11

UCB/EERC-81/08 "The Undrained Shearing Resistance of Cohesive Soils at Large Deformations," by M.R. Pyles and H.B. Seed - August 1981

UCB/EERC-81/09 "Experimental Behavior of a Spatial Piping System with Steel Energy Absorbers Subjected to a Simulated Differential Seismic Input," by S.F. Stiemer, W.G. Godden and J.M. Kelly - July 1981

UCB/EERC-81/10 "Evaluation of Seismic Design Provisions for Masonry in the United States," by B.I. Sveinsson, R.L. Mayes and H.D. McNiven - August 1981 (PB82 166 075)A08

UCB/EERC-81/11 "Two-Dimensional Hybrid Modelling of Soil-Structure Interaction," by T.-J. Tzong, S. Gupta and J. Penzien - August 1981(PB82 142 118)A04

UCB/EERC-81/12 "Studies on Effects of Infills in Seismic Resistant R/C Construction," by S. Brokken and V.V. Bertero - September 1981 (PB82 166 190)A09

UCB/EERC-81/13 "Linear Models to Predict the Nonlinear Seismic Behavior of a One-Story Steel Frame," by H. Valdimarsson, A.H. Shah and H.D. McNiven - September 1981(PB82 138 793)A07

UCB/EERC-81/14 "TLUSH: A Computer Program for the Three-Dimensional Dynamic Analysis of Earth Dams," by T. Kagawa, L.H. Mejia, H.B. Seed and J. Lysmer - September 1981(PB82 139 940)A06

UCB/EERC-81/15 "Three Dimensional Dynamic Response Analysis of Earth Dams," by L.H. Mejia and H.B. Seed - September 1981 (PB82 137 274)A12

UCB/EERC-81/16 "Experimental Study of Lead and Elastomeric Dampers for Base Isolation Systems," by J.M. Kelly and S.B. Hodder - October 1981 (PB82 166 182)A05

UCB/EERC-81/17 "The Influence of Base Isolation on the Seismic Response of Light Secondary Equipment," by J.M. Kelly - April 1981 (PB82 255 266)A04

UCB/EERC-81/18 "Studies on Evaluation of Shaking Table Response Analysis Procedures," by J. Marcial Blondet - November 1981 (PB82 197 278)A10

UCB/EERC-81/19 "DELIGHT.STRUCT: A Computer-Aided Design Environment for Structural Engineering," by R.J. Balling, K.S. Pister and E. Polak - December 1981 (PB82 218 496)A07

UCB/EERC-81/20 "Optimal Design of Seismic-Resistant Planar Steel Frames," by R.J. Balling, V. Ciampi, K.S. Pister and E. Polak - December 1981 (PB82 220 179)A07

UCB/EERC-82/01 "Dynamic Behavior of Ground for Seismic Analysis of Lifeline Systems," by T. Sato and A. Der Kiureghian - January 1982 (PB82 218 926)A05

UCB/EERC-82/02 "Shaking Table Tests of a Tubular Steel Frame Model," by Y. Ghanaat and R. W. Clough - January 1982 (PB82 220 161)A07

UCB/EERC-82/03 "Behavior of a Piping System under Seismic Excitation: Experimental Investigations of a Spatial Piping System supported by Mechanical Shock Arrestors and Steel Energy Absorbing Devices under Seismic Excitation," by S. Schneider, H.-M. Lee and W. G. Godden - May 1982 (PB83 172 544)A09

UCB/EERC-82/04 "New Approaches for the Dynamic Analysis of Large Structural Systems," by E. L. Wilson - June 1982 (PB83 148 080)A05

UCB/EERC-82/05 "Model Study of Effects of Damage on the Vibration Properties of Steel Offshore Platforms," by F. Shahrivar and J. G. Bouwkamp - June 1982 (PB83 148 742)A10

UCB/EERC-82/06 "States of the Art and Practice in the Optimum Seismic Design and Analytical Response Prediction of R/C Frame-Wall Structures," by A. E. Aktan and V. V. Bertero - July 1982 (PB83 147 736)A05

UCB/EERC-82/07 "Further Study of the Earthquake Response of a Broad Cylindrical Liquid-Storage Tank Model," by G. C. Manos and R. W. Clough - July 1982 (PB83 147 744)A11

UCB/EERC-82/08 "An Evaluation of the Design and Analytical Seismic Response of a Seven Story Reinforced Concrete Frame - Wall Structure," by F. A. Charney and V. V. Bertero - July 1982(PB83 157 628)A09

UCB/EERC-82/09 "Fluid-Structure Interactions: Added Mass Computations for Incompressible Fluid," by J. S.-H. Kuo - August 1982 (PB83 156 281)A07

UCB/EERC-82/10 "Joint-Opening Nonlinear Mechanism: Interface Smeared Crack Model," by J. S.-H. Kuo - August 1982 (PB83 149 195)A05

UCB/EERC-82/11 "Dynamic Response Analysis of Techi Dam," by R. W. Clough, R. M. Stephen and J. S.-H. Kuo - August 1982 (PB83 147 496)A06

UCB/EERC-82/12 "Prediction of the Seismic Responses of R/C Frame-Coupled Wall Structures," by A. E. Aktan, V. V. Bertero and M. Piazza - August 1982 (PB83 149 203)A09

UCB/EERC-82/13 "Preliminary Report on the SMART 1 Strong Motion Array in Taiwan," by B. A. Bolt, C. H. Loh, J. Penzien, Y. B. Tsai and Y. T. Yeh - August 1982 (PB83 159 400)A10

UCB/EERC-82/14 "Shaking-Table Studies of an Eccentrically X-Braced Steel Structure," by M. S. Yang - September 1982

UCB/EERC-82/15 "The Performance of Stairways in Earthquakes," by C. Roha, J. W. Axley and V. V. Bertero - September 1982 (PB83 157 693)A07

UCB/EERC-82/16 "The Behavior of Submerged Multiple Bodies in Earthquakes," by W.-G. Liao - Sept. 1982 (PB83 158 709)A07

UCB/EERC-82/17 "Effects of Concrete Types and Loading Conditions on Local Bond-Slip Relationships," by A. D. Cowell, E. P. Popov and V. V. Bertero - September 1982 (PB83 153 577)A04

UCB/EERC-82/18 "Mechanical Behavior of Shear Wall Vertical Boundary Members: An Experimental Investigation," by M. T. Wagner and V. V. Bertero - October 1982 (PB83 159 764)A05

UCB/EERC-82/19 "Experimental Studies of Multi-support Seismic Loading on Piping Systems," by J. M. Kelly and A. D. Cowell - November 1982

UCB/EERC-82/20 "Generalized Plastic Hinge Concepts for 3D Beam-Column Elements," by P. F.-S. Chen and G. H. Powell - November 1982

UCB/EERC-82/21 "ANSR-III: General Purpose Computer Program for Nonlinear Structural Analysis," by C. V. Oughourlian and G. H. Powell - November 1982

UCB/EERC-82/22 "Solution Strategies for Statically Loaded Nonlinear Structures," by J. W. Simons and G. H. Powell - November 1982

UCB/EERC-82/23 "Analytical Model of Deformed Bar Anchorages under Generalized Excitations," by V. Ciampi, R. Eligehausen, V. V. Bertero and E. P. Popov - November 1982 (PB83 169 532)A06

UCB/EERC-82/24 "A Mathematical Model for the Response of Masonry Walls to Dynamic Excitations," by H. Sucuoğlu, Y. Mengi and H. D. McNiven - November 1982 (PB83 169 011)A07

UCB/EERC-82/25 "Earthquake Response Considerations of Broad Liquid Storage Tanks," by F. J. Cambra - November 1982

UCB/EERC-82/26 "Computational Models for Cyclic Plasticity, Rate Dependence and Creep," by B. Mosaddad and G. H. Powell - November 1982

UCB/EERC-82/27 "Inelastic Analysis of Piping and Tubular Structures," by M. Mahasuverachai and G. H. Powell - November 1982

UCB/EERC-83/01 "The Economic Feasibility of Seismic Rehabilitation of Buildings by Base Isolation," by J. M. Kelly - January 1983

UCB/EERC-83/02 "Seismic Moment Connections for Moment-Resisting Steel Frames," by E. P. Popov - January 1983

UCB/EERC-83/03 "Design of Links and Beam-to-Column Connections for Eccentrically Braced Steel Frames," by E. P. Popov and J. O. Malley - January 1983

UCB/EERC-83/04 "Numerical Techniques for the Evaluation of Soil-Structure Interaction Effects in the Time Domain," by E. Bayo and E. L. Wilson - February 1983

UCB/EERC-83/05 "A Transducer for Measuring the Internal Forces in the Columns of a Frame-Wall Reinforced Concrete Structure," by R. Sause and V. V. Bertero - May 1983